The CARMEn project: A sustainable and circular brine treatment chain

Desalination 621 (2026) 119641

Contents lists available at ScienceDirect

Desalination

journal homepage: www.elsevier.com/locate/desal

The CARMEn project: A sustainable and circular brine treatment chain

Giuseppe Scelfo [a,b], Giuseppe Battaglia [a,*], Michela Cardella [a], Antonella Filingeri [b], Andrea Culcasi [a], Francesco Volpe [a], Lorenzo Craveri [c], Erica Bertozzi [c], Alberto Tiraferri [c], Giorgio Micale [a]

[a] Università degli Studi di Palermo, Dipartimento di Ingegneria, Viale delle Scienze, 90128, Palermo, PA, Italy
[b] ResourSEAs S.r.L, Via Notarbartolo 38, 90141, Palermo, PA, Italy
[c] Politecnico di Torino, Corso Duca degli Abruzzi, 24, 10129, Torino, TO, Italy

HIGHLIGHTS

- A novel treatment chain for valorisation of waste saline solutions was introduced.
- Laboratory tests with RO brine, NF retentate and saltworks bitterns proved the idea.
- A techno-economic analysis assessed the viability of the chain at a pilot plant.
- Waste heat coupling boosted the economic viability of the chain.
- The lowest Levelized cost of $Mg(OH)_2$ of 1320 €/ton was calculated.

GRAPHICAL ABSTRACT

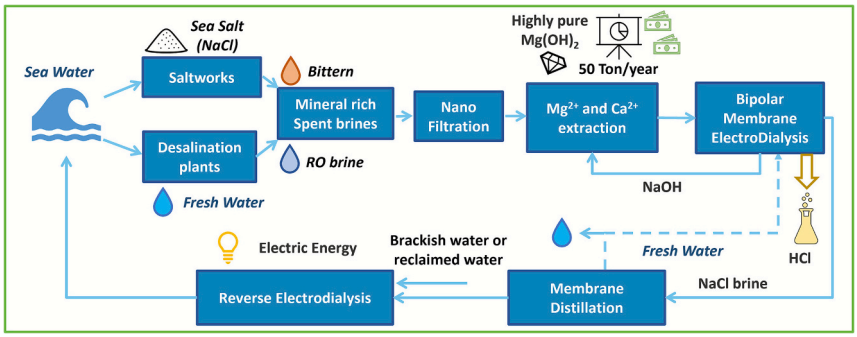

ARTICLE INFO

Keywords:
Mineral and water recovery
Circular approaches
Water treatment
Magnesium hydroxide
Brine valorization

ABSTRACT

The increasing demand for water and critical minerals is currently largely met through linear processes, such as desalination and saltworks, which generate highly saline waste streams typically discharged to the sea. These brines, however, are rich in valuable components. The Italian-funded CARMEn project proposes a circular approach to valorize such streams by producing magnesium hydroxide, freshwater, and energy through an integrated treatment chain. As proof of concept, real reverse osmosis (RO) brine and saltworks bitterns were processed at laboratory scale through a sequence of nanofiltration, reactive precipitation, softening, electrodialysis with bipolar membranes, membrane distillation, and reverse electrodialysis. Experimental data supported the development of a preliminary techno-economic analysis to assess the viability of a pilot plant targeting 50 tons/year of $Mg(OH)_2$. Results show that feed composition and operating pH strongly influence performance. Bitterns, with Mg^{2+} concentrations ~20 times higher than RO brine, led to the lowest CAPEX and EnEx and enabled >99.7 % product purity, but required external water input, reducing circularity. RO brine and NF retentate achieved full circular operation without external inputs, though with higher costs and slightly lower product purity (approximately between 85 and 93 %). Across all scenarios, EDBM and MD dominated energy demand, but coupling MD with waste heat reduced power consumption lowering the levelized cost of $Mg(OH)_2$.

* Corresponding author.
E-mail address: giuseppe.battaglia03@unipa.it (G. Battaglia).

https://doi.org/10.1016/j.desal.2025.119641
Received 7 October 2025; Received in revised form 10 November 2025; Accepted 14 November 2025
Available online 18 November 2025

1. Introduction

One of the main challenges faced today is the substantial population growth, which has led the global population to exceed 8 billion, with projections estimating an increase to 9.5 billion by 2050 [1]. This trend is driving a continuously rising demand for essential resources such as water, as well as for critical goods necessary for technological development, such as metals and minerals. To meet these demands, linear economic models have typically been adopted. A clear example of such linear approaches is the production of freshwater from seawater. Various technologies are available, including reverse osmosis (RO) [2–4] and electrodialysis (ED) [5,6] as membrane-based technologies, multi-effect distillation (MED) or mechanical vapor compression (MVC) as thermal processes [7,8] and hybrid approaches such as membrane distillation (MD) [9,10]. Globally, the most widely used desalination process is reverse osmosis (RO); indeed, more than two-thirds of desalination plants worldwide employ this technology [11]. The RO process produces freshwater (with a water recovery factor typically <50 % [12]), but also generates an equal to or greater amount of waste brine (the RO retentate), usually discharged back into the sea. Although different disposal methods have been proposed, many are not sustainable due to potential environmental impacts [13,14].

Another example of linear processes is sea salt production in saltworks. Specifically, sea salt is harvested through natural evaporation processes in shallow evaporation ponds, located in coastal regions, where climatic conditions are optimal for continuous seawater evaporation, such as high solar radiation, steady winds, and low humidity [15]. As evaporation proceeds, its chemical composition gradually changes [16] and the least soluble salts, such as calcium carbonate ($CaCO_3$) and calcium sulfate ($CaSO_4$), precipitate [17]. In the final stages, the solution reaches saturation with sodium chloride (NaCl), initiating its crystallization. The residual liquid, called bittern, is saturated in NaCl and enriched in ions such as magnesium and potassium. It is generally discharged as waste, although it represents a valuable source of elements.

To meet the world demand while guaranteeing a sustainable, resilient economy, production processes must become more efficient and circular [18], following the circular economy concept. This approach extends product lifecycles, minimizes waste, supports a more sustainable and regenerative system [18], educes resource extraction, thereby enhancing material value and societal resilience [19]. Driven by these principles, several innovative treatment chains have been proposed. For example, the European funded SEArcularMINE project proposed an integrated treatment chain to valorize bitterns through the recovery of magnesium, lithium and trace elements, e.g., boron and strontium [20,21].

In this context, the Italian-funded CARMEn project aims at developing a novel circular approach to produce high-added-value compounds (notably magnesium hydroxide), green energy, and freshwater from RO brine and saltworks bitterns. Magnesium, especially in form of hydroxide, is of particular interest owing to its broad industrial applications, including as: i) flame retardant [22], ii) neutralizing agent for wastewater and acid gas treatment [23], as well as anti-aging in the paper industry [24]. Moreover, it can also be employed in several CO_2 sequestration schemes through carbonation [25]. Fig. 1 shows a schematic representation of the CARMEn treatment chain for the recovery of magnesium hydroxide.

The process is designed to utilize three primary feed streams: (i) the RO brine, (ii) a stream obtained from a nanofiltration (NF) unit treating the RO brine (referred to as NF retentate), and (iii) saltworks bitterns. The NF process plays a crucial role in the selective concentration of divalent ions present in the RO brine. These ions, especially Mg^{2+}, Ca^{2+}, Sr^{2+}, SO_4^{2-}, are highly rejected and enriched in the retentate [26], whose flow rate is typically 30–40 % [27] of that of the feed. The RO brine, the NF retentate or the bittern are processed separately in the subsequent step: a reactive precipitation reactor. Here, the addition of an alkalizing agent triggers controlled precipitation of two key products: magnesium hydroxide ($Mg(OH)_2$) and/or calcium hydroxide ($Ca(OH)_2$) [28]. The reactor produces two streams: a solid-rich slurry and a clarified solution. The solids exit the treatment chain, while the clarified solution is sent to

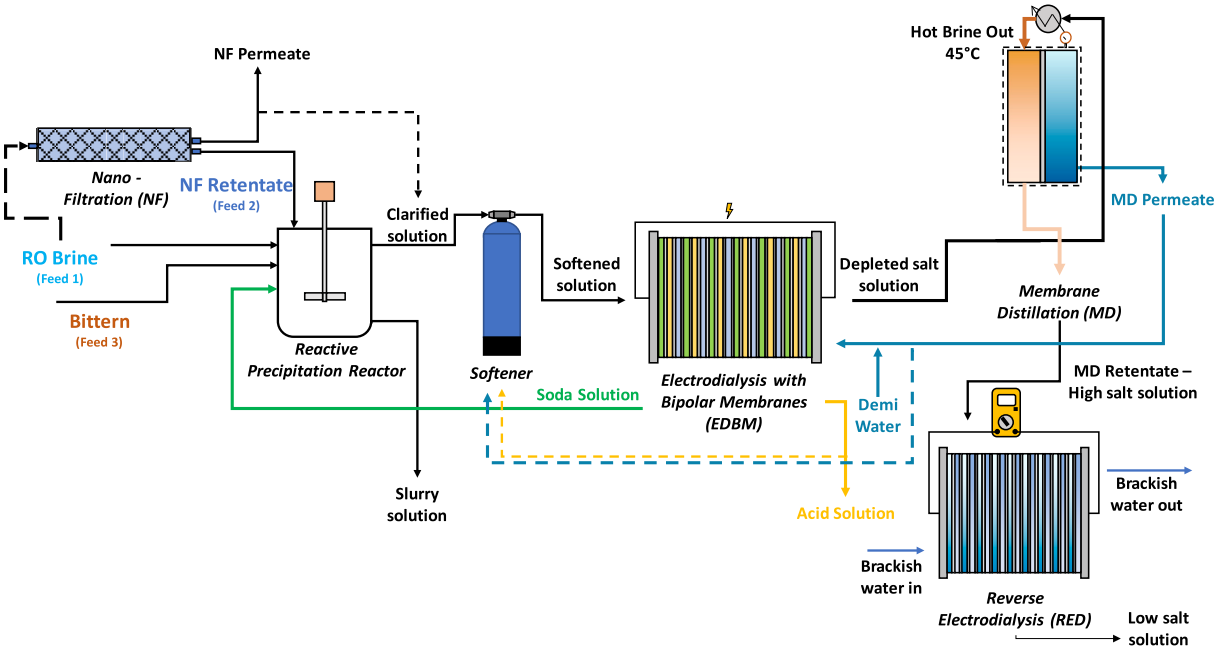

Fig. 1. Schematic representation of the CARMEn treatment chain. Three alternative feed streams, reverse osmosis (RO) brine, nanofiltration (NF) retentate, and saltworks bittern, are directed to a precipitation reactor for magnesium hydroxide recovery. The clarified stream undergoes softening and is then treated by electrodialysis with bipolar membranes (EDBM), producing soda (recycled to the reactor) and acid (used for resin regeneration). The depleted saline solution is concentrated in a membrane distillation (MD) unit, which provides high-purity water for reuse, while the remaining high-salinity brine is valorized in a reverse electrodialysis (RED) unit to generate electrical power. The integration of precipitation, softening, EDBM, MD, and RED enables the simultaneous recovery of $Mg(OH)_2$, freshwater, and energy within a circular treatment chain.

a softening unit to remove residual divalent ions and minimize scaling in downstream units. The softened stream then enters an electrodialysis with bipolar membrane (EDBM) unit. Here, the salinity of the feed and demi-water streams is exploited to generate both acid and base solutions, via an electrochemical system composed of cation-exchange, anion-exchange, and bipolar membranes under an applied electric field [29]. The basic stream is recycled to the crystallization reactor to support continuous precipitation reactions, while the acidic one is partially used to regenerate the softener. Following the EDBM process, the depleted salt solution proceeds to a membrane distillation (MD) unit. Using moderate heat and, in some cases, vacuum, water vapor passes across a hydrophobic membrane, driven by a vapor pressure gradient. The vapor condenses on the cooler permeate side, yielding a purified distillate that is recirculated to the EDBM, reducing freshwater demand [30]. The remaining brine, highly concentrated in monovalent salts, is a valuable input for reverse electrodialysis (RED), where it is paired with a low-salinity stream, namely, brackish water, to drive ionic migration across ion-selective membranes, thereby generating electrical energy [31]. The system consists of alternating cation- and anion-exchange membranes stacked between electrodes. Ionic transport from the high- to the low-salinity stream is converted into electrical current and harvested through an external load. The mixed outlet solutions from the RED unit reach an overall ionic concentration close to that of seawater, thus their disposal into the sea does not raise environmental concerns. The entire chain is highly integrated, enabling circular use of water, energy, and chemicals.

In the present work, this treatment train is validated at laboratory scale using real RO brine from the Lampedusa desalination plant and real bittern from the Trapani saltworks, under multiple feed conditions. These streams, intrinsically rich in valuable resources such as salts, water, and chemical energy, are processed to demonstrate how each unit operation contributes to their valorization. Experimental results support the development of a preliminary techno-economic model of a pilot plant designed to produce 50 tons/year of $Mg(OH)_2$. The article first describes the design and operating principles of the integrated chain, then presents a techno-economic analysis of different scenarios, with all assumptions and input data for the analyses being supported by laboratory findings on $Mg(OH)_2$ recovery and stream characterization, as detailed in the Appendix. Together, these results provide proof-of-concept and assess the viability of transforming saline effluents from desalination and saltworks into valuable products, high-purity $Mg(OH)_2$, freshwater, and renewable energy, through a fully integrated and circular approach. It is worth noting that, commercial $Mg(OH)_2$ solids are typically produced from magnesium-bearing sources, such as bischofite brines (Aman process), serpentinite (Magnifin process) and magnesite ores. Aman and Magnifin processes rely on pyrohydrolysis (800–900 °C) of $MgCl_2$-containing solutions to generate high purity crude magnesium oxide, which is then hydrated into $Mg(OH)_2$. These processes require a high energy demand, causing a high CO_2 release, both from fuel burning and the CO_2 amount contained in the minerals. Luong et al. [32] reported estimated greenhouse gas (GHG) emissions of 1.6–3.3 kg CO_2-eq/kg $Mg(OH)_2$ treating a bischofite brine and 2.6–5.2 kg CO_2eq/kg $Mg(OH)_2$ from serpentinite ore, clearly highlighting a drastic environmental impact reduction through the use of aqueous brines. In this context, the present work introduces a production chain for highly pure $Mg(OH)_2$ solids from rejected brines (no ores consumption) at low temperature and pressure, expecting to contribute to the reduction of environmental impacts of the $Mg(OH)_2$ manufacturing chain.

2. Materials and methods

2.1. Simplified modeling of the treatment chain unit

The entire treatment chain was modeled using a simplified approach based on regression analyses of laboratory-scale experiments (Appendix A) and literature data. This methodology enabled system performance to be estimated under various conditions by correlating key operational parameters with observed outcomes, offering a practical and data-driven model of the treatment process.

On this basis, a techno-economic model of the process was developed at pilot scale. For this purpose, both capital expenditure (CAPEX) and energetical expenditure (EnEx) were included in the analysis.

CAPEX cost was estimated using the six-tenths rule [33] as shown in Eq. (1):

$$C_2[€] = C_1\left(\frac{A_2}{A_1}\right)^{0.6} \tag{1}$$

where C_2 is the cost referred to the new capacity, A_2, and C_1 is the cost for the known capacity, A_1. This equation could not be applied to the MD unit because, given its low technology readiness level (TRL), no clear or sufficient up-scaled examples are present. The total cost of the MD unit was therefore estimated from the specific cost of the membranes.

To estimate the electrical consumption to pumping the solution within the units the following equation was used:

$$P[kW] = \frac{Q_{feed}\Delta P}{\eta \cdot 1000} \tag{2}$$

where Q_{feed} is the inlet flowrate (m^3/s), ΔP is the static head provided by a pump (Pa), η is the working efficiency of the pump, fixed here at a value of 70 %. The factor 1000 accounts for the conversion of the power unit in kW. For each unit, the specific electric consumption, apart from the pumping one, is discussed in the following sections.

2.1.1. Nanofiltration

The nanofiltration unit is designed to concentrate divalent ions (i.e., magnesium) in the main saline stream, while allowing most monovalent ions to pass through the membrane. Two key performance parameters are used to characterize and design the process. The rejection factor, R_{NF}, expresses the ability of the NF process to retain different salts and is specific for each salt:

$$R_{NF} = 1 - \frac{c_p}{c_f} \tag{3}$$

where c_p and c_f are the concentration of salt (e.g., $MgSO_4$ or NaCl) in the permeate and feed streams, respectively. The second key performance indicator is the recovery rate of the unit, defined as the ratio of the flowrate of permeate solution to the flowrate of the supplied feed water:

$$Rec_{NF} = 1 - \frac{Q_{perm_{NF}}}{Q_{feed_{NF}}} \tag{4}$$

where $Q_{perm_{NF}}$ and $Q_{feed_{NF}}$ are the flowrates of permeate and feed streams to the NF unit, respectively.

The rejection rates were assumed to match the values reported in the supplier's technical datasheet; see Table A2. The same rejection coefficients applied to magnesium and sodium, respectively, were also applied to the calcium and potassium ions. A recovery rate of 50 % was adopted, consistent with literature data [34] and in good agreement with experimental data reported in Section A.3.1 of Appendix A.

The total membrane area of the NF unit, A_{NF}, was calculated as the ratio between the retentate flow needed to achieve the target production of 50 tons of $Mg(OH)_2$ per year, and the operating flux, i.e., $A_{NF} = Q_{feed_{NF}}/J_{NF}$. A design flux of 11 L/m^2h, derived from experimental tests and considered representative for scale-up, was assumed (see Fig. A6).

2.1.2. Precipitation reactor

The goal of this unit was to recover the main divalent cations, such as Ca^{2+} and Mg^{2+}, in the form of hydroxides through the addition of an alkaline solution and pH control. The reactions in play were the following (see Eqs. (5) and (6))

$$Mg^{2+} + 2\,OH^- \rightarrow Mg(OH)_2(s) \quad (5)$$

$$Ca^{2+} + 2\,OH^- \rightarrow Ca(OH)_2\,(s) \quad (6)$$

The precipitation reactions of calcium and magnesium hydroxides occur at characteristic pH values, dictated by their solubility. Therefore, the pH at which precipitation begins can be calculated using the solubility product constant (K_{sp}). As an example, Eq. (7) gives the solubility product of $Mg(OH)_2$ [35]:

$$K_{sp_{Mg(OH)_2}} = \left[Mg^{2+}\right]\left[OH^-\right]^2 \quad (7)$$

Given the $K_{sp_{Mg(OH)_2}}$ value of 1.5×10^{-11} [mol^3/L^3] (at 25 °C), the equilibrium pH of 10.35 is found while, the equilibrium pH for the $Ca(OH)_2$ is equal to 12.4, given the $K_{sp_{Ca(OH)_2}}$ value of 7.6×10^{-6}. In order to promote magnesium conversion, an excess of hydroxyl ions, or a higher pH, should be applied to drive the reaction toward the effective formation of the product. In the techno-economic analysis, a correlation between Mg^{2+} conversion and reaction pH was adopted based on literature and experimental data, as described in Table B2 of Appendix B.

Given the chemical composition of the feed solutions (see Table A1), the possible co-precipitation of calcium carbonate ($K_{sp_{CaCO_3}} = 3.3\,10^{-9}\ mol^2/L^2$ at 25°C) must be considered:

$$Ca^{2+} + CO_3^{2-} \rightarrow CaCO_3(s) \quad (8)$$

The precipitation of calcium carbonate is a well-known issue when recovering $Mg(OH)_2$ species from seawater RO brines [36]. It is also worth specifying that, also the formation of magnesium carbonate may occur, however its high solubility in water $K_{sp_{25°C}} = 2.6\,10^{-5} mol^2/L^2$, makes such phenomenon unlikely.

2.1.3. Divalent cation removal unit (softener)

This unit was designed for the removal of the main divalent cations remaining in the clarified solutions after solids settling. These residual cations can cause scaling issues in the downstream units. [39]. For the purpose of modeling, a Purolite SSTC104 resin [37] was chosen. This material is characterized by a high exchange capacity for divalent ions (4.7 eq/L, or 2.35 mol/L [37]) and ensures long saturation times. The volume of the required resin, V_{resin}, computed through Eq. (9), was designed to guarantee a continuous functioning of the unit for at least one month.

$$V_{resin} = \frac{Q_{cla} * C_{div} * 660}{0.75 * 2.35} \quad (9)$$

Here, Q_{cla} and C_{div} are the volumetric flow rate (L/h) and the molar concentration (mol/L) of divalent species in the softener unit, respectively; the factor 660 accounts for a monthly operating condition of the resins, i.e., one twelfth of 8000 h (typical industrial yearly working hours); the coefficient 2.35 is the sorption capacity of the resin (mol/L resin), while 0.75 is a safety factor applied to avoid fully saturation of the resin and, thus, losses of traces of divalent cation.

To regenerate the resin, an acid stream flow through. To carry out the regeneration process, 4.7 equivalents of H^+ per liter of resin must be supplied. Accordingly, the required acid flowrate to be diverted from the acid stream produced by the EDBM unit (at a certain H^+ concentration, H^+_{conc}), was determined as shown in Eq. (10):

$$Q_{acid_{Soft}} = \frac{4.7 * V_{resin}}{H^+_{conc} * 660} \quad (10)$$

To complete the procedures required for resin regeneration, a volume of water equal to 4 bed volumes (BV) was needed to carry out the brine displacement, acid displacement, and resin rinsing phases. This water, where possible, was supplemented by drawing a flow of permeate from the downstream MD unit. The water demand of resin was computed through Eq. (11):

$$Q_{water_{Soft}} = \frac{4 * V_{resin}}{660} \quad (11)$$

2.1.4. Electro-dialysis with bipolar membrane (EDBM)

The goal of the EDBM unit was to produce the chemicals (i.e., the alkaline and acid solution) needed by the treatment chain using saline solutions from upstream units. The molar flow rate, $\dot{M}$ [mol/h], of acid and base produced by the system, see Eq. (12), depends on several factors, including the applied current density i [A/m^2], the number of repeating units (triplets), N_t, and the current efficiency, CE, is the latter parameter that indicates the fraction of electric charge effectively converted into ionic species. Size and the geometric shape of the channels are those reported in a previous work for a semi-industrial scale EDBM plant [38]. Specifically, the active membrane area, the spacer width and the spacer thickness were 0.32 m^2, 0.19 m and 760 μm, respectively.

$$\dot{M} = Q_{soda} C_{soda} = Q_{acid} C_{acid} = \frac{i\,A_{act}\,CE\,N_t\,3600}{F} \quad (12)$$

where Q_i and c_i are the acid and base flowrate [L/h] and molar concentration [mol/h] respectively. F is the Faraday constant equal to 96,485.3C/mol, and the coefficient 3600 accounts for unit conversion. The current density in this analysis is fixed at the value of 200 A/m^2, in accordance with laboratory experimental conditions (Appendix A).

A final parameter considered in the analysis is the recycle flow rate imposed in the system to ensure adequate velocity in the channels, set at 0.1 m/s as indicated in the technical datasheet provided by the supplier. This flowrate (m^3/h) is therefore calculated as shown in the following Eq. (13):

$$Q_{rec_{EDBM}} = \left(0.1 \cdot \tau_{spacer} \cdot w \cdot N_t\right) \cdot 3600 \quad (13)$$

In Eq. (13) the product $\tau_{spacer} \cdot w$ represents the cross-section area of the channels, the coefficient 0.1 is the fixed velocity imposed in the channels. This flowrate is equal across all three hydraulic circuits (acid, base and salt).

For CAPEX and EnEx estimation, the number of triplets was varied to match the required acid or alkaline flowrate of the plant. However, a limit of 300 triplets per unit was imposed, due to technological limits. Therefore, if more than 300 triplets were requested, a second EDBM unit was considered in the analysis. Moreover, it is important to highlight that not all ions in solutions can be converted into acid and base. A small concentration of salts, $C_{salt_{out}}$ (assumed at 0.05 M of equivalent NaCl), should remain in solution to prevent a significant increase in stack resistance. On these bases, the maximum soda molar flowrate was computed as follows Eq. (14):

$$Q_{soda} C_{soda} = Q_{salt_{in}} C_{salt_{in}} - Q_{salt_{out}} C_{salt_{out}} \quad (14)$$

Regarding the electric consumption of the unit, the stack resistance, $R_{stack_{EDBM}}$, accounts for the sum of electrical resistance of the electrodes, those of the membranes, and those of the electrolyte solutions. The total EDBM power consumption, P_{EDBM}, was calculated by Eq. (15):

$$P_{EDBM} = \left(\frac{Q_{feed_{EDBM}} + Q_{soda} + Q_{acid}}{1000 * 3600 * \eta}\right)\Delta P_1 + \left(\frac{3 \cdot Q_{rec_{EDBM}}}{3600 * \eta}\right)\Delta P_2 + R_{stack_{EDBM}}\left(i * A_{act}\right)^2 \quad (15)$$

where $Q_{feed_{EDBM}}$ is the flow rate [L/h] of the saline solution coming from the softener unit, η is the pumping efficiency, imposed to be 0.7, while ΔP_1 and ΔP_2 are the pressure losses of the feed and recirculation hydraulic circuits, being 0.25 and 1 bar, respectively. The values of $R_{stack_{EDBM}}$ are reported in Appendix B.

2.1.5. Membrane distillation (MD)

The primary goal of membrane distillation was to extract clean water from the saline solution exiting the EDBM unit by using a hydrophobic membrane that allows only water vapor to pass through, while retaining

and thus concentrating the salt in the retentate. The inlet temperature (T_{in}) in this unit was 445°C (following the one adopted in the experimental tests, see Appendix A), while the outlet (T_{out}) was 25°C due to expected higher heat losses at pilot scale. To achieve the target temperature, the feed stream is heated in a heat exchanger to reach the target operating temperature. This process is also illustrated in Fig. 2.

The key performance parameters for this unit were water recovery and, consequently, the concentration factor, defined as follows:

$$Rec_{MD} = \frac{\dot{Q}_{perm_{MD}}}{\dot{Q}_{feed_{MD}}} \cdot 100 \tag{16}$$

$$Concentration\ Factor = \frac{\dot{Q}_{feed_{MD}}}{\dot{Q}_{ret_{MD}}} \tag{17}$$

Based on laboratory data (Section A.3.4), a concentration factor of 5 was imposed, corresponding to a water recovery of 80 %. Moreover, salt rejection was assumed to be 100 %, consistent with experimental values >99.8 % (see Section A.3.4). At laboratory scale, a permeate flux of approximately 4 $L{\cdot}m^{-2}h^{-1}$ was obtained. For scale-up, a conservative design flux of 1.5 $L{\cdot}m^{-2}\ h^{-1}$ was assumed to account for operational limitations [39]. Based on this flux value, the membrane area was calculated to achieve the target water recovery of 80 %.

2.1.6. Reverse electrodialysis

Reverse electrodialysis (RED) is an electrochemical process that generates electricity by exploiting the salinity gradient between two solutions, typically brine and a diluted salty solution. In the RED unit, the flow rates were controlled in order to achieve specific velocities within the membrane channels: 0.5 cm/s for the high salinity and 1.0 cm/s for the low salinity ones (see Appendix A). To ensure the desired velocity within the channels, the number of cell pairs was accordingly determined, see Eq. (18),

$$N_{cell\ pair} = \frac{Q_{high\ solution_{RED}}}{v_{high\ solution_{RED}} * \tau_{channel_{RED}} * w_{channel_{RED}}} \tag{18}$$

in which $Q_{high\ solution_{RED}}$ and $v_{high\ solution_{RED}}$ are the flow rate and the fluid velocity of the high salinity in the RED unit, respectively, $\tau_{channel_{RED}}$ and $w_{channel_{RED}}$ represent the thickness (fixed value equal to 0.00027 m as the lab scale unit) and width (equal to 0.8 m), of the unit, respectively. In the calculations, $v_{high\ solution_{RED}}$ was imposed to be 0.5 cm/s as used in laboratory tests. Once the number of cell pairs was determined, the flow rate of the diluted solution required achieving the target velocity of 1 cm/s was calculated.

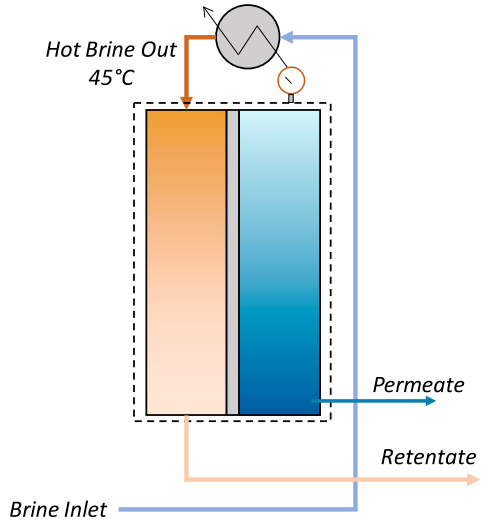

Fig. 2. Membrane distillation (MD) scheme and heat recovery unit.

To estimate the electric potential generated by the interaction between the two solutions within the unit, the Open Circuit Voltage (OCV) was calculated as shown in Eq. (19):

$$OCV = N_{cell\ pair}\ \alpha_{ave} \frac{2RT}{zF} ln\left(\frac{C_{high}\gamma_{high}}{C_{low}\gamma_{low}}\right) \tag{19}$$

In Eq. (19), α_{ave} represents the average permselectivity of the anion and cation membranes, set to an average value of 0.95. The activity coefficients, γ_i, were estimated using the Pitzer model, implemented through the PhreeQC simulation platform assuming that the entire TDS (Total Dissolved Solids) content of the solutions was solely attributed to sodium chloride. Note that Pitzer model can be adopted for saline solutions with TDS up to ~290 g/L (~5.0 M of NaCl) [40].

A second estimated parameter is the stack resistance, computed as the sum of the electrode resistance (namely blank resistance) and the whole cell pair resistance, computed as the product of specific cell pair resistance and the number of cell pair, as shown in the following Eq. (20):

$$R_{stack} = R_{blank} + N_{cell\ pair} R_{cell\ pair} \tag{20}$$

From the laboratory data, a constant blank resistance (R_{blank}) of 0.247 Ω was used in the model, along with a specific cell pair resistance $R_{cell\ pair}$ of 0.46 Ω, as reported in Table A10. The working assumption, as discussed in the Appendix B, was to operate under an external load that provides an external resistance (R_{load}) equal to R_{stack} in order to maximize the produced power density of the unit and then the whole generation of power. Under this assumption, the maximum power generation was given by Eq. (21):

$$P_{max} = \frac{OCV^2}{4\ R_{stack}} \tag{21}$$

Note that, for the sake of simplicity, the maximum power generation was adopted in the model without considering the non-Ohmic phenomena occurring in the stack. In fact, neglecting non-ohmic effects, the stack resistance can be considered constant under any current condition; consequently, the maximum power output is mathematically achieved when the load resistance equals the stack resistance.

2.2. Reference values

The CARMEn project adopts, in several cases, unconventional or non-industrial technologies such as EDBM, MD and RED ones. For these membrane processes, it was assumed that the membrane lifespan was five years and the membrane cost accounted for 30 % of the total unit cost. In order to carry out the techno-economic analysis the following reference capital costs for pilot scale units were considered:

- A capital cost of €76,000 for a NF pilot unit equipped with 94.8 m^2 of installed membrane area [41]. Considering the membrane lifespan of 5 year, the NF CAPEX is then estimated as Eq. (22) while the EnEx of unit was solely associated with pumping energy which was evaluated through Eq. (2).

$$NF_{CAPEX} = 76000 \left(\frac{A_{NF}}{94.8}\right)^{0.6} \left(1 + 0.3 * \frac{Chain\ Lifetime - Memb.Lifetime}{Memb.Lifetime}\right) \tag{22}$$

- A capital cost of €82,000 for 20.7 L $Mg(OH)_2$ crystallizer [42], considering a residence time of 0.125 h, as suggested by Ventimiglia et al. for high settling and filtration rates suspensions [36]. EnEx was estimated taking into account the consumption of feed and recirculation pumps, considering the recirculation flowrate to be 20 times higher than the sum of the inlet flowrates, and a static head of 0.5 bar to overcome pressure drops in the recirculation line.

- A capital cost of €20,000 for 100 L of resin for the Softener unit [42]. The energy consumption was assumed to be equal to 0.4 kWh/m^3 of treated solution [43] while the acid and water consumption for the elution phases are those explained in Eqs. (10)–(11).
- A capital cost of €150,000 for a 48.75 m^2 (50 triplet of 0.975m^2 each) EDBM unit. The price was scaled by the number of triplets installed in the unit, considering 400 triplets as a maximum target. Considering the membrane lifespan of 5 year, the CAPEX of the EDBM was then estimated as Eq. (23):

$$EDBM_{CAPEX} = 150000\left(\frac{N_{triplet}}{50}\right)^{0.6}\left(1+0.3*\frac{ChainLifetime-Memb.Lifespan}{Memb.Lifespan}\right) \quad (23)$$

The EDBM unit also involved water consumption, as water was fed into the acid and base channels to generate the corresponding solutions. In this simplified analysis, non-ideal phenomena that could cause volume variations were not considered; therefore, the water consumption was assumed to be equal to the flow rate of the produced acid and base solutions. The electrical consumption of the unit was evaluated through Eq. (15).

- To estimate the capital cost of the MD unit a specific membrane cost of 100 €/m^2 was assumed [44]. Since the membrane typically accounts for about the 30 % of the total cost of the unit, and considering the lifespan of the membrane, the CAPEX of the MD unit was estimated using the following formula:

$$MD_{CAPEX} = \frac{A_{MD}[m^2]*100\left[\frac{€}{m^2}\right]}{0.30}\left(1+0.3*\frac{Chain\ Lifetime-Memb.Lifespan}{Memb.Lifespan}\right) \quad (24)$$

Regarding the electrical consumption of the unit, two contributions were considered: (i) a fixed electrical demand for feed and recirculation pumps, and (ii) the thermal power required to heat the feed to the target temperature. In the latter case the equivalent electrical power, related to the thermal one with a conversion factor equal to 3 (3 kW_{th} equal to 1 kW_{el}), was taken into account. In this regard, this last contribution, P_{MD}, was calculated by Eq. (25):

$$P_{MD} = Q_{feed_{MD}}\rho_{feed_{MD}}\cdot cp_{feed}\cdot\left(T_{in_{MD}} - T_{feed}\right) \quad (25)$$

In Eq. (25), $Q_{feed_{MD}}$, $\rho_{feed_{MD}}$, and cp_{feed} are the flow rate [L/h], the density [g/L] and the specific heat (4.05 kJ/kgK) of the feed inlet solution, respectively, while $T_{in\,MD}$ and T_{feed} represent the feed temperature after preheating (45 °C) and the initial feed temperature (25 °C). Specific heat values were chosen according to the average NaCl concentration of the solutions (0.3 M for the feed and 1.5 M for the retentate). Regarding the electrical consumption of the MD unit, the power demand was assumed to be calculated following Eq. (2) in which the flowrate was the sum of the feed flowrate and the recirculation one (the latter assumed to be 10 time higher the feed flowrate). The imposed ΔP was 0.5 bar.

Regarding the MD configuration, commercial-scale modules are currently based on Air gap MD (AGMD) or vacuum air-gap MD (V-AGMD) configurations, given that these two configurations are the most effective for real-scale systems. In the present study, the available laboratory module was a direct contact MD (DCMD) unit that ensures reliable and reproducible operation without the complexity associated with vacuum and air-gap system operation and maintenance. It is also worth noting that Winter et al. [45] reported data for a 27.5 m^2 DCMD module, showing that DCMD can be up-scaled to membrane areas that is comparable to that of current AGMD and V-AGMD commercial modules.

- Based on the experience of the research group, a capital cost of €12,500 for a RED unit of 3.2 m^2 of installed membrane area in 20 cell pair, i.e., active membrane area of 0.08 m^2, was considered. The price was scaled, using Eq. (1), by a total membrane area calculated as the product between 0.08 m^2 (the area of the pilot unit discussed above) and the total number of cell pairs estimated from Eq. (18). A number of 500 cell pairs was the maximum imposed for each RED stack, as shown in the literature [46,47]. Thus, if necessary, other RED units, working in parallel, were adopted (split of area) to achieve the target. The power requirement by the unit was the energy fed to the two feed pumps. Based on laboratory data, the ΔP was fixed at 0.25 bar for the concentrated stream and 0.50 bar for the diluted stream. The required power input was therefore calculated using Eq. (2). However, the total unit energy demand was fully or partially met by the electric power generated in loco.

It is worth noting that many of the technologies are still at demonstration scale, with research activities devoted to their industrial scale-up and application. MD scale-up is challenged by several factors, including energy requirements, polarization phenomena, membrane wetting and fouling, and overall long-term operation stability. The main limitation of large-scale MD system is their high thermal energy demand, as larger modules tend to exhibit higher conductive heat losses through the membrane [48]. This issue can be mitigated by coupling the process with waste heat or other low-grade energy sources, such as solar thermal energy [49,50]. Temperature polarization effects become more pronounced in real-size systems compared to laboratory conditions, thus reducing the overall driving force of the process [51,52]; permeate fluxes are therefore significantly lower compared to those observed at small scale. Membrane wetting and fouling also represents major concerns, as they can compromise the membrane properties and the product quality, particularly when operating with high salinity feed streams [53,54]. Despite these challenges, several studies have demonstrated the feasibility of MD at the pilot scale, highlighting that successful scale-up can be achievable under optimized system design and operating conditions [55,56]. Concerning RED units, it is well known that the power density of RED units decreases in large-scale units with large membrane areas and longer flow paths, due to salinity gradient depletion along the channel length. However, an upscaled setup allows for higher energy conversion and more efficient resources utilization, thus enhancing the total power output of the unit with lower operating costs [58]. Membrane fouling and membrane properties deterioration, both of which affecting membrane lifetime, are also two crucial parameters for pilot-scale systems. Fouling has been extensively investigated in laboratory units (e.g. 10 × 10 cm^2 membrane area), while few studies have reported data for large-scale units. However, it should be note that, Tedesco et al. successfully operated the first full-scale RED unit with natural hypersaline streams for a period of 5 months without significant detrimental performance over time [59] thanks to the use of a proper pre-treatment stage, i.e. cartridge filters and shock treatment with hypochlorite.

Table 1 summarizes the reference CAPEX cost for all units.

2.3. Levelized cost of $Mg(OH)_2$

In order to compare different system configurations from an economic point of view, the concept of Levelized Cost (LC) was introduced. The levelized cost is a financial metric that calculates the cost of the treatment chain over its lifetime, assumed here to be 20 years, divided by the total amount of produced product, the magnesium hydroxide. The LC effectively combines capital expenditure and operating costs into

Table 1
Reference CAPEX costs adopted in the economic analysis for all units of the CARMEn project.

	NF	CRISTALLYZER	SOFTENER	EDBM	MD	RED
A_1	94.8 m^2	20.7 L	100 V_{resin}	50 Triplet	1 m^2	3.2 m^2
C_1 [€]	76,000	82,000	20,000	150,000	100	12,500

a single value, enabling straightforward comparison across alternatives. For the purposes of this analysis, the LC was calculated under the following simplifying assumptions:

- Linear depreciation of CAPEX. The initial capital investment (CAPEX) was assumed to be evenly depreciated over a period of 20 years, regardless of the actual technical lifetime of the system.
- Only two operating costs were considered: electricity consumption with a relative cost, $Elec_{cost}$, of 0.2 €/kWh [60] and a water cost, namely Wat_{cost}, equal to 0.66 €/m^3 [62]. Other operational expenditures, such as maintenance, cost of labor or waste disposal were intentionally excluded at this stage.
- All the produced acid, exceeding the amount of acid needed to elute the softening column, is a by-product and, assuming an average price of 75 €/ton [63], it was computed as revenue. Dilute hydrochloric acid solutions (concentration below 1 M) are often employed for chemical cleaning and rinsing procedures without causing significant corrosion or material degradation. In addition, the low content of impurities, e.g. salts and sulphates, makes the acidic stream suitable for a wide range of uses, such as RO cleaning procedures, where a pH close to 2 is maintained [64]. Worth noting also that a low-concentration acid stream avoids the amount of water required for dilution of concentrated commercial ones (33 %w/w).

The Levelized Cost ($LC_{Mg(OH)_2}$) was thus evaluated through Eq. (26) in which EnEx cost and water recovery was calculated considering 8000 h as annual working hours.

$$LC_{Mg(OH)_2} = \left(\frac{CAPEX\ [€]}{20\ [years]} + \left\{\left[\left(EnEx\ [kW]{*}Elec_{cost}\left[\frac{€}{kWh}\right] - Water\ Rec\left[\frac{m^3}{h}\right]{*}Wat_{cost}\left[\frac{€}{m^3}\right]\right){*}8000\left[\frac{h}{year}\right]\right] - \left[\left(Q_{acid_{EDBM}}\left[\frac{L}{h}\right]{*}8000\left[\frac{h}{year}\right] - Q_{acid_{Soft}}\left[\frac{L}{month}\right]{*}12\left[\frac{month}{year}\right]\right){*}H^+_{conc}\left[\frac{mol}{L}\right]{*}PM_{HCl}\left[\frac{g}{mol}\right]{*}10^{-6}{*}75\left[\frac{€}{Ton}\right]\right]\right\}\right) \Big/ \frac{1}{Mg(OH)_2\ Prod\ \left[\frac{Ton}{year}\right]} \quad (26)$$

3. Results and discussion

Productivity analyses were carried out based on a fixed annual production target of 50 tons of magnesium hydroxide. The assessment was conducted considering three different pH conditions (10.6–12–12.5), as tested experimentally (see Appendix A), to evaluate the impact of reaction conditions on the overall plant performance. Reaction pH affects key operational parameters such as the purity of Mg $(OH)_2$ powders and the net water production of the process. Specifically, the net production was defined as the difference between the amounts of freshwater produced by the MD unit and that required by the EDBM and softener unit. To ensure consistency across scenarios, a fixed soda concentration of 1 M was assumed. This soda was produced in situ using the EDBM unit, operated at a current efficiency of 60 %. As a result, any differences observed between scenarios, despite variations in pH, can be more clearly attributed to process conditions. Nevertheless, the case using the lower soda concentrations adopted in the laboratory-scale tests (Appendix A) is also presented, to allow direct comparison with experimental results.

3.1. Productivity analysis

3.1.1. RO brine as feed stream

To achieve the target $Mg(OH)_2$ production of 50 ton/y, 1.349, 1.305 and 1.302 m^3/h of RO brine were used for the pH values of 10.6, 12, and 12.5, respectively. Solutions were directly fed into the precipitation reactor without being treated through the NF unit. An excess soda flowrate, relative to the stoichiometric requirement, equal to 0.5 %–35.4 %–47.8 %, was supplied by the EDBM unit to reach the desired final pH values. Based on RO brine and NaOH flow rate, and considering the fixed residence time of 0.125 h in the reactor, presented above, the reactor volume was calculated to be 202.9, 207, and 211.4 L, respectively. In addition to the targeted $Mg(OH)_2$ productivity, by-product formation of calcium carbonate was observed at 3.81, 3.68 and 3.67 ton/year. The $CaCO_3$ fraction affected the purity of $Mg(OH)_2$ solids, yielding values between 92.9 and 85.6 %, in accordance with experimental data reported in Appendix A. The softening unit was considerably affected by the reaction pH due to the residual amount of divalent ions. The required resin volume was 9.1, 7.4, and 4.4 m^3 for the three respective cases, reflecting the lower Ca^{2+} amount at higher pH values. To meet the soda demand across the process chain, the EDBM system required 188, 245, and 267 triplets, with corresponding power consumptions of 16.8, 21.9, and 23.9 kW. Treatment of the depleted saline solution from the EDMB in the MD unit required active membrane areas of 779.1, 796.5, and 881.9 m^2 (corresponding to 30, 31 and 34 modules of 26 m^2 MD pilot units, the biggest MD modules available in the market), targeting a net water production of 0.57, 0.44, and 0.41 m^3/h in the three cases. These targets were achieved with electrical heating demands of 14.44, 14.70, and 14.92 kW, respectively. At the end of the process chain, the RED unit was installed with a total active area of 96.2, 98.4, and 100.2 m^2, achieving gross power outputs of 0.096, 0.106, and 0.098 kW, respectively. The overall CAPEX of the chain was 1.92, 2.02, and 2.01 million euros for the three scenarios, while the overall EnEx in terms of electrical power consumption reached 32.61, 38.00, and 40.24 kW, respectively. Details of the CAPEX and EnEx distributions are shown in Figs. 3 and 4.

As shown in Fig. 3, the capital cost of the softener unit gradually decreases with increasing pH, reflecting the higher recovery of divalent ions in the precipitation step. This reduces the divalent load on the softener column, ultimately resulting in a smaller volume of resin. Conversely, the capital cost of the EDBM unit increased due to the higher number of repeating units needed to meet the increased soda production demand. Specifically, a 23 % increase in EDBM CAPEX cost is observed when the pH was raised from 10.6 to 12.5. A slight increase in capital cost is also observed for the reactor unit, primarily due to the larger volume needed to accommodate the higher soda flow required for pH adjustment. A similar trend is noted for the RED unit, which also showed a marginal cost increase.

Regarding the distribution of energy costs, EDBM and MD clearly dominate across all scenarios, confirming their role as the most energy-intensive steps responsible for water and chemical recovery. As the pH increased, the electrical energy consumption of the MD and EDBM unit also increased due to the higher power required to heat the feed solution to the target temperature. Minor increases in reactor and softener energy costs were also observed, primarily linked to higher pumping requirements at elevated solution flow rates.

These trends are consistent with the current TRL of the units: MD is still at low TRL and therefore represents one of the main CAPEX drivers, while EDBM, even if it has an intermediate TRL, is the dominant contributor. The EnEx cost of the MD unit was high due to the

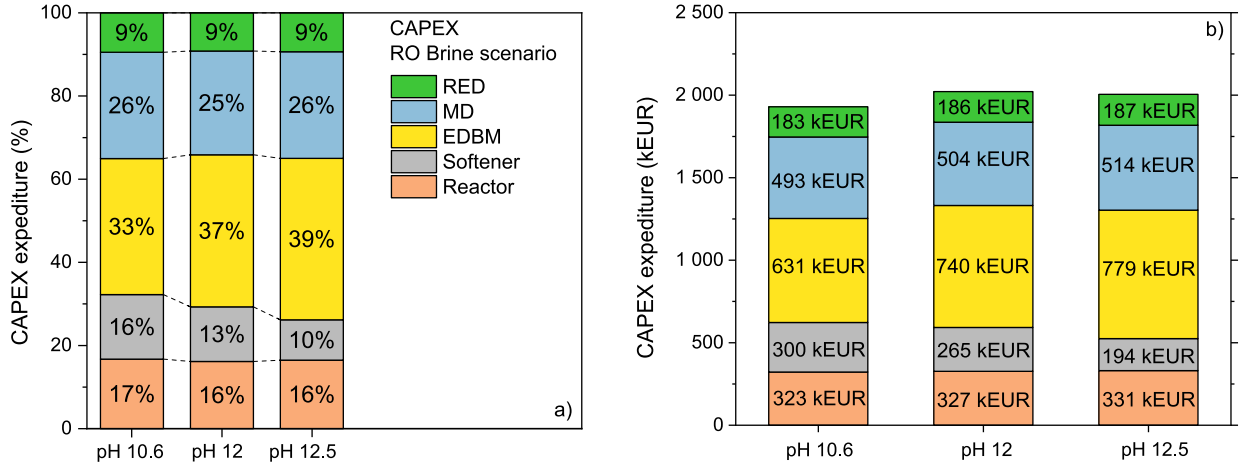

Fig. 3. Capital expenditure (CAPEX) distribution for the RO brine scenario at three different reaction pH values (10.6, 12, and 12.5). The pie charts show the relative contributions of the main units of the treatment chain: membrane distillation (MD), electrodialysis with bipolar membranes (EDBM), precipitation reactor, softener, and reverse electrodialysis (RED). Increasing the reaction pH reduced the CAPEX share of the softener due to enhanced precipitation of divalent ions, while the relative cost of the EDBM unit was higher because of the higher demand for soda production. MD consistently accounted for the largest share of CAPEX across all cases, reflecting the comparatively low TRL of this technology relative to the other units.

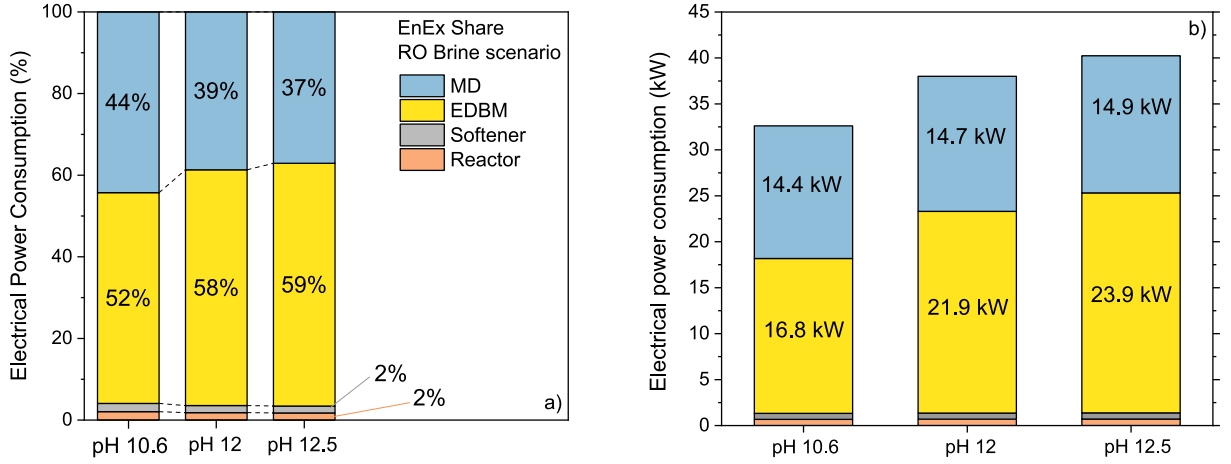

Fig. 4. Distribution of electrical power consumption for the RO brine scenario at three different reaction pH values (10.6, 12, and 12.5). The pie charts show the relative contributions of the main units: membrane distillation (MD), electrodialysis with bipolar membranes (EDBM), precipitation reactor, and softener. MD consistently accounted for share of electrical demand (37–44 %), while EDBM contributed 52–59 %. The reactor and softener consumed only marginal amounts (<2 %), highlighting that MD and EDBM are the dominant energy-intensive steps of the chain.

intrinsically high energy demand of this high-salinity separation step and because it was assumed to be provided through electrical heating. As discussed below, this process becomes more economically and environmentally sustainable when driven by low-grade heat sources. Softening and precipitation reactors are mature, low-cost technologies, explaining their marginal shares. RED, although at a low TRL, contributes little to both CAPEX and EnEx in this configuration because of the modest scale of energy recovery modeled here. This alignment reinforces the credibility of the modeling results and highlights that reducing MD costs and energy demand is the key step for improving the overall viability of the chain.

3.1.2. NF retentate as feed stream

To achieve the target $Mg(OH)_2$ productivity, 1.391, 1.343, and 1.342 m^3/h of RO brine were fed into the NF unit to obtain 0.695, 0.672, and 0.671 m^3/h of NF retentate. As previously noted, the NF system generates a retentate stream enriched in divalent ions and a permeate stream mostly free of them. Since membranes do not possess perfect selectivity and due to the relatively high recovery rate, a portion of salts was transferred to the permeate stream. Pumping to the target pressure of 68 bar required 4.23 kW of electrical power. To recover the divalent cation, soda produced by the EDBM unit was supplied in the reactor with an excess over the stoichiometric flowrate equal to 0.5 %, 35.4 %, and 47.8 %. To maintain the specified residence time and treat the reduced flowrate compared to the RO brine, smaller reactor volumes of 121.2, 128.5, and 132.5 L were required. Volumes were almost half of those calculated for the RO brine case due to the almost double concentration of Mg^{2+} in the NF retentate stream. Precipitated $Mg(OH)_2$ solids had purities between 92.6 % and 85.4 %, limited by $CaCO_3$ precipitation, To meet the salt requirements of the EDBM for acid and base production, 25 % of the NF permeate stream, rich in NaCl, was mixed with the clarified solution from the reactor and softened. This fraction was selected as a compromise between ensuring sufficient salt availability in the EDBM unit and minimizing the additional MD membrane area required to treat larger solution volumes. The required resin volume ranged between 9.04 m^3 and 4.4 m^3 as pH increased. The EDBM unit required the same number of triplets as in the RO brine case but consumed less power (16.48, 21.47 and 23.40 kW) due to reduced electrical resistance after mixing NF permeate with clarified reactor effluent.

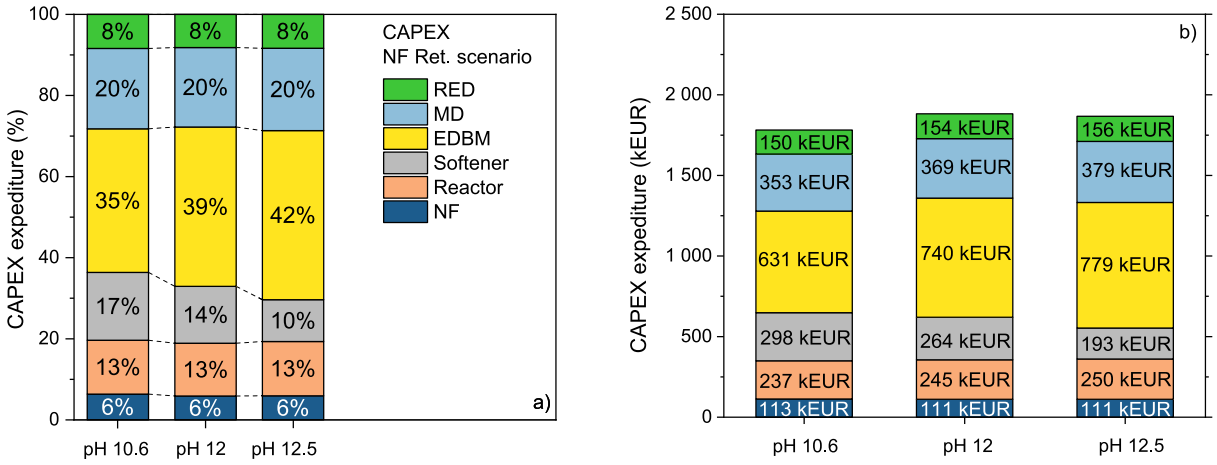

Fig. 5. Capital expenditure (CAPEX) distribution for the NF retentate scenario at three different reaction pH values (10.6, 12, and 12.5). The pie charts show the contributions of the main units: nanofiltration (NF), membrane distillation (MD), electrodialysis with bipolar membranes (EDBM), precipitation reactor, softener, and reverse electrodialysis (RED). The NF unit introduced an additional cost (~6 % of CAPEX), while MD and EDBM remained the dominant contributors.

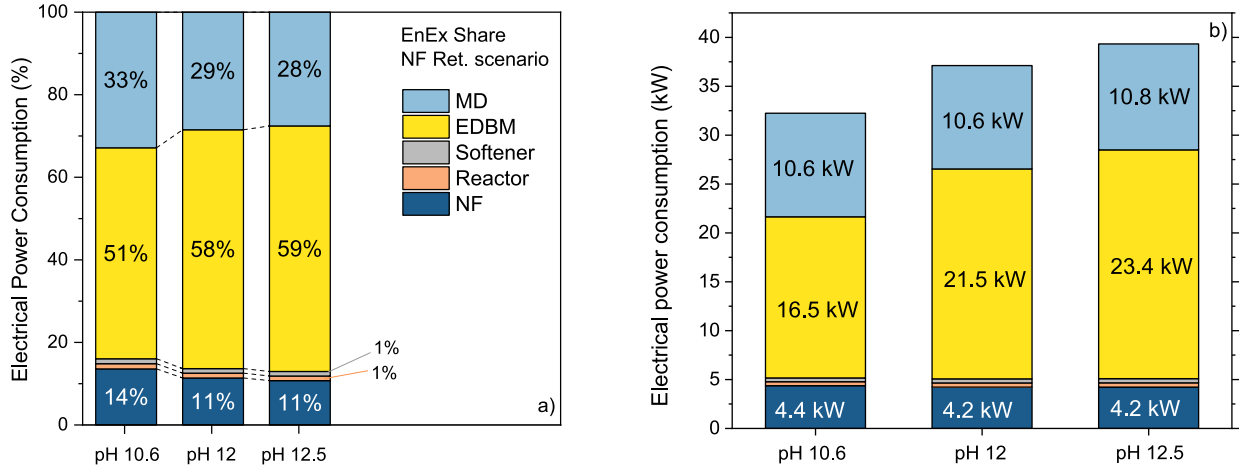

Fig. 6. Distribution of electrical power consumption for the NF retentate scenario at three different reaction pH values (10.6, 12, and 12.5). EDBM and MD dominated across all cases, while NF accounted for 11–14 % of total demand, making it the third most energy-intensive step. The reactor and softener remained marginal contributors (<1 %). Compared with the RO brine case, MD power consumption was ~30 % lower due to reduced volumes owing to the NF separation.

The active membrane area of the MD unit was 557.9, 583, and 598.5 m^2, respectively, (22–23 pilot units in parallel), with electrical heating demands of 10.59, 10.58 and 10.84 kW. The RED unit had a total active area of 68.8, 72, and 73.8 m^2, delivering an average gross power outputs of ~0.046 kW. The overall CAPEX was 1.78, 1.88, and 1.87 million euros, while the EnEx were 32.23, 37.12, and 39.33 kW (electrical power consumption), respectively. Net water demand in the three scenarios was 0.24, 0.12, and 0.09 m^3/h. CAPEX and EnEx share costs were shown in Figs. 5 and 6.

In this scenario, an additional capital cost was introduced by the NF unit, which serves to concentrate the RO retentate in divalent ions. Its contribution to overall CAPEX is limited, representing only ~6 % of total costs. A similar trend to the RO brine case (Fig. 3) is observed in the NF scenario.

Energy cost trends also remained consistent with those observed in the RO brine case. However, in this configuration, the NF unit accounted for approximately 11–14 % of the total electricity consumption, making it the third most energy-intensive unit in the system. Overall energy consumption by EDBM and MD was reduced, primarily due to lower processing volumes enabled by the increased magnesium concentration in the feed, which lowered pumping power requirements and reduced thermal energy demand in the MD unit. Notably, the MD unit showed a substantial reduction in required electrical power, with approximately 30 % lower energy costs compared to the RO brine scenario. The same considerations made for the RO brine scenario and aligning TRL with costs of the unit may be made.

3.1.3. *Saltworks bittern as feed stream*

In the case of saltworks bitterns, 0.058, 0.053, and 0.052 m^3/h of bittern was fed into the system. As discussed above and reported in the Appendix A, the NF unit could not be applied to concentrate this solution; therefore, was excluded from this scenario. To evaluate the three pH cases, soda was dosed at the stoichiometric flowrate with excess additions of 0.3 %, 19.3 %, and 26.1 %. The corresponding reactor volumes were 36.5, 38.8 and 40.5 L, respectively. The purity of the solids was >99 % due to the low concentration of Ca^{2+}, resulting in $CaCO_3$ formation of only about 0.15, 0.139, and 0.13 ton/year. Note that, due to the very low concentration, in most cases, traces of Ca^{2+} were lower than limit of quantification. Purity of powders was confirmed by experiments described in Section A.3.2. The required resin volumes in the softener were 3.5, 0.11, and 0.05 m^3 for the three pH cases, reflecting the near-absence of Ca^{2+} in the bittern. By contrast, in RO brine and NF retentate streams, only part of Ca^{2+} precipitates in the reactor, with the remainder requiring removal downstream. To meet the

soda demand, the EDBM system required 161, 177, and 186 triplets, with associated electrical consumptions of 14.1, 15.1 and 15.9 kW, respectively. The active area of the MD unit was 140.2, 148.9, and 155.6 m^2, achieving water production rates of 0.378, 0.408, and 0.429 m^3/h, respectively. These outputs were obtained with electrical energy requirements of 2.53, 2.66 and 2.77 kW. However, due to the limited inlet flow, the treatment chain required external demineralized water supplies of 0.28, 0.29, and 0.31 m^3/h, corresponding to negative net water production. At the end of the process chain, the RED unit required a total active area of 17.3, 18.4, and 19.2 m^2, delivering gross power outputs of 0.025, 0.015, and 0.013 kW, respectively.

A total CAPEX of 1.06, 0.91, and 0.93 million euros were estimated, with EnEx in terms of electrical power consumption of 16.82, 18.06, and 19.04 kW, respectively. CAPEX and EnEx share costs are shown in Figs. 7 and 8.

Once again, also in the case of bittern processing, the investment cost trends mirrored those observed in the previous scenarios, with higher pH increasing costs due to its influence on magnesium conversion and on the operating requirements of the EDBM and MD units.

3.1.4. Comparison among analysis results

Fig. 9 summarizes the main economic and process outputs for the three saline solutions investigated at different pH values. The distinct Mg^{2+} concentration in the feed streams considerably influenced CAPEX, as shown in Fig. 9a. In fact, bittern was almost 20 times more concentrated in magnesium ions with respect to the RO brine, thus requiring substantially lower equipment volumes (or flow rates, in this context). With NF pretreatment, a more concentrated magnesium solution was processed compared to the RO brine scenario, lowering the volume of equipment size and thus the CAPEX costs. Overall, the CAPEX evaluated for the bittern case was almost one half that of RO brine or NF retentate. For RO brine and NF retentate, CAPEX increased with pH, peaking at 12, mainly due to the higher number of EDBM triplets and the greater MD membrane area needed to supply additional permeate. Conversely, in the bittern scenario, raising pH reduced CAPEX, largely due to a reduced softener cost (lower resin amount).

The energy consumption of the treatment chain clearly rose as the reaction pH increased. Specifically, values of 32.61 kW, 32.23 kW, and 16.82 kW at pH 10.6 increased to 40.24 kW, 39.33 kW, and 19.04 kW at pH 12.5 in the case of the RO brine, NF retentate and bittern, respectively; see Fig. 9.b. In the NF retentate scenario, despite the presence of the energy-intensive NF unit and larger feed volume processed by the MD unit (due to the recirculation of the NF permeate), the overall energy consumption remained lower compared to that of the RO brine case. The bittern configuration required lower the energy of the other two scenarios, owing to the lower flowrates and reduced pumping needs.

One of the most relevant aspects may be the net water recovery, shown in Fig. 9c. In the RO and NF solution cases, the integration of MD technology allowed for the generation of sufficient permeate to support the production of both acid and base streams within the EDBM unit and the regeneration of the softening resins. This enables a fully circular treatment chain relying solely on brine and external power supply. Conversely, in bittern scenarios, a net negative water balance was observed, meaning that MD permeate production was insufficient to cover needs. As a result, an additional external supply of demineralized water was required. This not only introduces an extra operational cost, but also compromises the full circularity of the process.

The purity of $Mg(OH)_2$ solids, presented in Fig. 9d, ranged between 85 % and 93 % in the RO brine and NF retentate cases, reaching values greater than 99.5 % in the bittern-based scenarios, reflecting its negligible Ca^{2+} content. Solid production (Fig. 9e) shows that $Mg(OH)_2$ output was consistently fixed at 50 tons/year, while calcium carbonate by-product ranged between 3.7 and 4 tons/year, reaching higher values at higher pHs, in the case of RO brine and NF retentate, while it was ~0.14 tons/year in the bittern case. The effect of pH on product purity was crucial, especially when the pH exceeded 12.4 in the RO and NF scenario for which the precipitation of calcium hydroxide is expected. Note that experimental data did not report any precipitation of $Ca(OH)_2$ species. This can be explained by a competitive mechanism in which calcium carbonate precipitation predominated over calcium hydroxide formation.

3.2. Influence of the NaOH concentration

In this section, the influence of the NaOH concentration is discussed by considering the effective NaOH solution concentrations adopted in the experimental campaign. For this reason, only the RO brine and NF retentate cases were analyzed.

3.2.1. RO brine

Results obtained from simulations using the laboratory-scale conditions in the case of the RO brine are reported in Table 2 and compared to those reported in Section 3.1.1. In this scenario, given the required low soda concentration, a current efficiency of 0.95 and 0.9 were assumed in the EDBM unit to produce soda solutions with molar concentrations of 0.171 M and 0.21 M, respectively.

Due to the lower concentration of the alkaline solution fed into the reactor, a higher soda flow rate is required to maintain the same

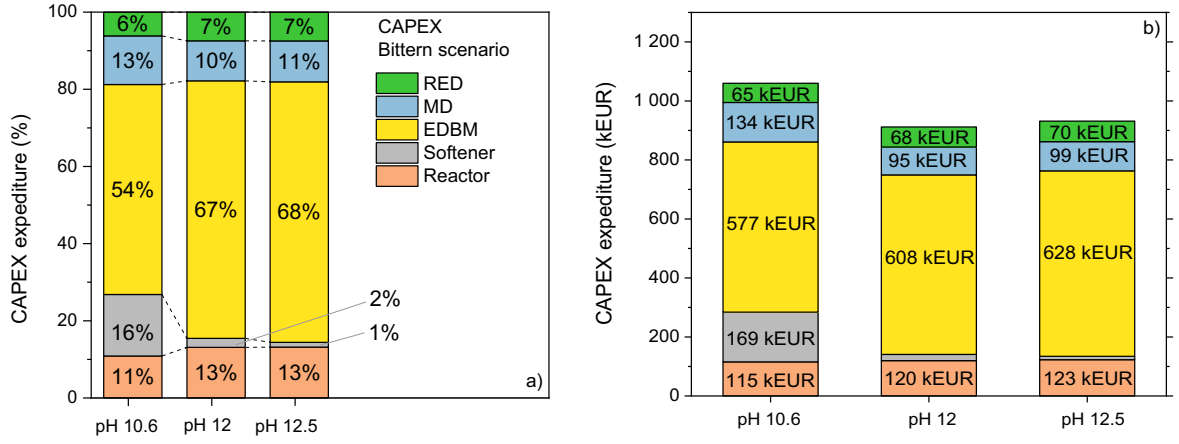

Fig. 7. Capital expenditure (CAPEX) distribution for the saltworks bittern scenario at three different reaction pH values (10.6, 12, and 12.5). The pie charts show the contributions of the main units: membrane distillation (MD), electrodialysis with bipolar membranes (EDBM), precipitation reactor, softener, and reverse electrodialysis (RED). EDBM consistently dominated CAPEX, while MD accounts for a smaller share than in the RO brine and NF retentate cases due to the lower flow rate handled.

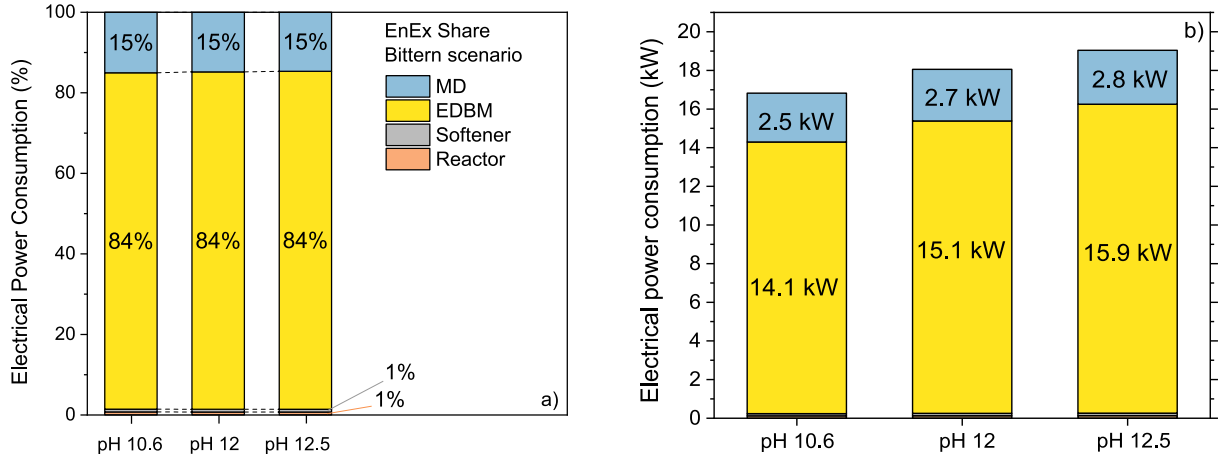

Fig. 8. Distribution of electrical power consumption for the saltworks bittern scenario at three different reaction pH values (10.6, 12, and 12.5). EDBM was the dominant energy consumer (≈84 % of total), while MD required considerably less power than in the other feed scenarios, due to reduced inlet flows. The reactor and softener remained negligible contributors (<1 %).

production rate. As a result, the reactor volume increased by a factor close to 40 %. On the other hand, because the EDBM was operated to produce more diluted acid and base streams, a higher current efficiency close to 95 % was assumed, which reduced the number of triplets required. Regarding the MD and RED units, the need to treat larger solution volumes increased unit sizes. Consequently, both capital and operating costs rose due to larger membrane area, higher pumping requirements and, in the case of MD, greater thermal energy consumption. Specifically, MD active area increased to ~1300–1400 m^2, corresponding to over 50 MD modules operating in parallel.

In the analysis, it can also be observed that water consumption is significantly higher under laboratory-scale conditions, primarily due to the greater amount of water required by the EDBM unit to produce diluted acid and soda solutions. Conversely, using a 1 M solution resulted in a net positive water production, thus closing the circularity of the plant, thus enabling full circularity of the process and improving both efficiency and economics.

3.2.2. NF retentate

Results obtained under laboratory-scale conditions for the NF retentate scenario, are reported in Table 3 and compared to those of Section 3.1.1. In this scenario, given the required soda concentration, current efficiencies of 0.85 and 0.75 were assumed or the production of soda concentrations of 0.31 M and 0.437 M, respectively.

As with RO brine, the lower soda concentration increased reactor volume and enlarged, MD and RED unit sizes. However, soda concentration had a positive impact on the EDBM due to the higher current efficiency, translating into a reduced number of EDBM triplets. Compared to the high-concentration case, CAPEX rose more moderately (+13 %), while net water recovery turned negative due to the higher water volumes required in the EDBM unit. Overall, the analysis marks the positive use of concentrated NaOH solution, both for RO brine and NF retentate scenarios, allowing mainly CAPEX to be reduced thanks to the lower volumes in the MD unit, while EnEx slightly varied due to EDBM current efficiency, which decreased increasing the concentration of the NaOH solution. In addition, a positive water recovery can be achieved with concentrated NaOH solutions.

3.3. Levelized cost of $Mg(OH)_2$

The levelized cost of magnesium hydroxide ($LC_{Mg(OH)_2}$), calculated with Eq. (26), is reported in Fig. 10. As expected, the $LC_{Mg(OH)_2}$ followed the same trend of CAPEX and electrical consumption. In the RO brine scenario, the CAPEX and EnEx costs due to high solution flowrates led to the highest $LC_{Mg(OH)_2}$ values, partially mitigated by the revenue from freshwater produced by the MD unit. Lower $LC_{Mg(OH)_2}$ values were found in the NF retentate scenario, the bittern scenario yielded the lowest values despite the need for external water addition. The $LC_{Mg(OH)_2}$ value agrees with that obtained by Scelfo et al. [42] for a similar treatment chain of bittern solutions. Nevertheless, $LC_{Mg(OH)_2}$ values remained well above market competitiveness. The reference price for highly pure magnesium hydroxide solids in the market is around 1000 €/ton [65], which is 40 % lower than the best scenario identified here. It should be emphasized, however, that these results were evaluated for a pilot scale; industrial-scale production is expected to yield significantly lower LC values.

3.4. Sensitivity analysis

A sensitivity analysis of the treatment chain was performed to assess the impact of the variation (up to 25 %) of (i) the electricity cost, (ii) the water cost, (iii) the selling price of the produced acid, (iv) the membrane lifespan, v) reactor cost and vi) softening resin cost. The analysis was carried out for the best operating conditions that had the lowest Levelized cost of $Mg(OH)_2$ identified in Section 3.3, namely RO brine and NF retentate at pH 10.6, and bittern at pH 12. The results of the sensitivity analysis are presented in Fig. 11.

Membrane lifespan and electricity costs were the main parameters affecting the Levelized Cost of $Mg(OH)_2$. A reduction of the lifespan of the membrane (from 5 to 3.75 years) led to an increase of the $LC_{Mg(OH)_2}$ of ~0.26 €/kg$Mg(OH)_2$, for the RO brine and NF retentate cases, and 0.16 €/kg$Mg(OH)_2$, for the bittern one, namely ~11 % with respect of the their $LC_{Mg(OH)_2}$ values, see Fig. 10. On the other hand, an increase in the membrane lifespan led only to a reduction of the $LC_{Mg(OH)_2}$ of about 6–7 %. The electricity cost increased or decreased the $LC_{Mg(OH)_2}$ of about ~10 %. The reactor and resin costs varied the $LC_{Mg(OH)_2}$ only by ±2–3 %, while acid and water costs had a negligible influence, i.e. ~0.5–1 %. An increase in the water cost positively affected the $LC_{Mg(OH)_2}$ in the case of RO brine and NF retentate, while negatively in the bittern case, in accordance with the positive net water recovery of RO and NF cases.

3.5. Waste heat coupling

The potential integration of waste heat was investigated as a means to supply the thermal demand of the MD unit. Such heat stream could originate from other industrial processes, such as waste heat stream from the cooling circuit of a power generation plant [66], or renewable systems (e.g., cooling water from concentrator photovoltaics [67,68]).

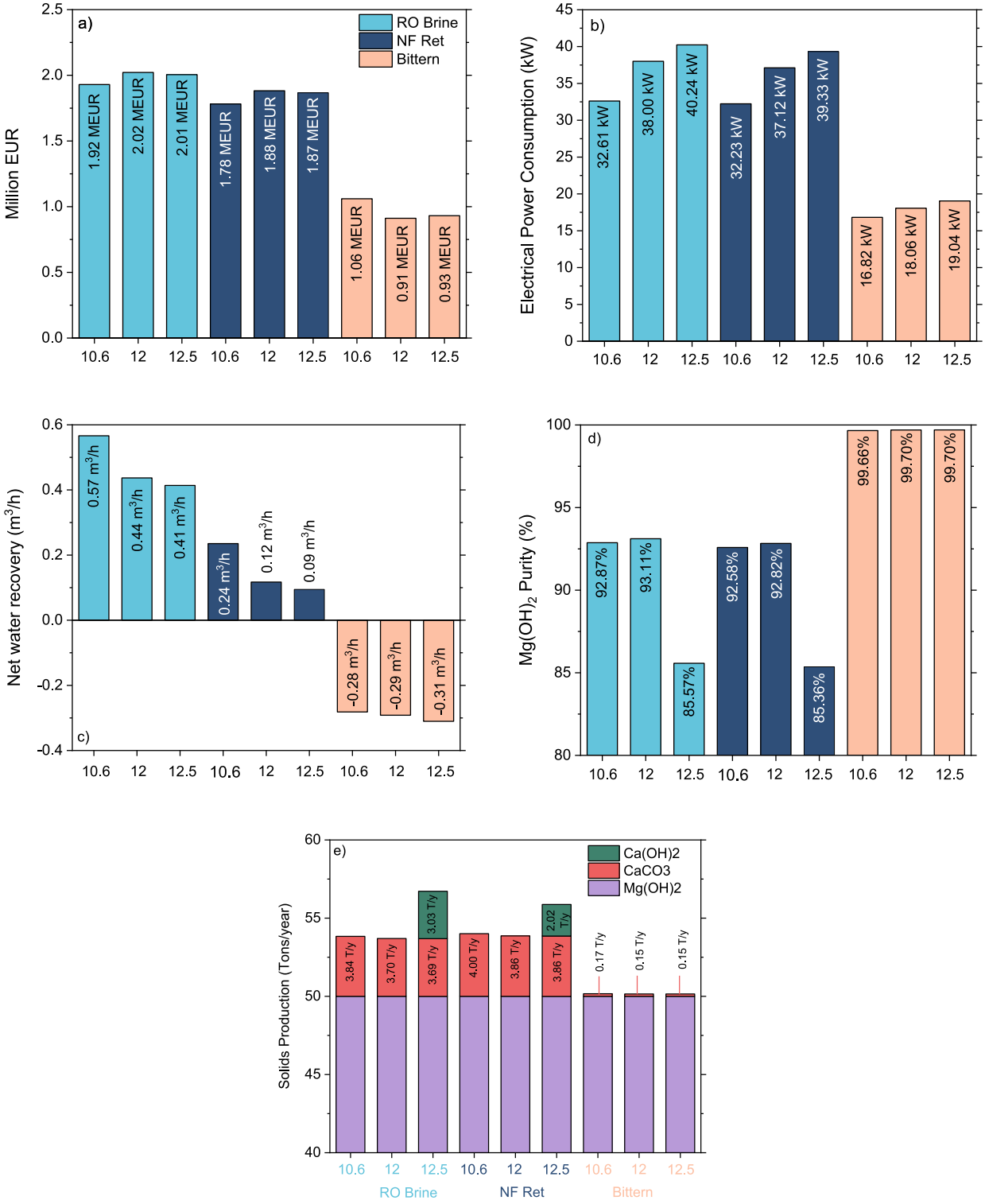

Fig. 9. Comparative summary of the three feed scenarios (RO brine, NF retentate, and saltworks bittern) at different reaction pH values. Panels show: (a) CAPEX, (b) electrical power consumption (EnEx), (c) net water recovery, (d) $Mg(OH)_2$ purity, and (e) solids production. Bittern scenarios exhibited the lowest CAPEX and EnEx and the highest product purity, but suffered from negative net water balances, requiring external water input. In contrast, RO brine and NF retentate cases enabled fully circular operation, though at higher costs and with lower product purity.

Under the assumption that the thermal energy was supplied entirely by waste heat, the electrical consumption and the $LC_{Mg(OH)_2}$ were re-evaluated, as shown in Fig. 12.

Electrical consumption was two thirds in the scenario involving brines where, MD energy demand accounted for 30 % - 40 % of the EnEx. Conversely, a smaller reduction was observed in the scenario involving bittern, since MD energy demand, accounting only for the 15 %, was strongly lower compared to the other cases. Despite the considerable power demand reduction, the $LC_{Mg(OH)_2}$ decreased by only roughly 20 %, because at pilot scale, CAPEX costs remain the dominant cost driver. Note that pilot-scale CAPEX is not fully representative of full-scale implementation. Importantly, in the bittern scenario, $LC_{Mg(OH)_2}$ values

Table 2
Comparison of unit size, CAPEX, EnEx, and water recovery between laboratory-scale operational conditions (experimental soda concentration) and simulated pilot-scale operational conditions (1 M soda) in the scenario involving RO brine as feed stream.

OH- Conc [M]	pH	Reactor [L]	Soft. resin [m^3]	EDBM [Triplet]	MD [m^2]	RED [m^2]	CAPEX [M€]	EnEx [kW]	Water rec [m^3]
0.171	10.6	378.6	9.16	125	1453.8	179.4	2.45	37.34	−1.24
1	10.6	202.9	9.16	188	779.1	96.2	1.93	32.61	0.57
0.210	12	354.2	7.49	140	1360.3	168	2.36	36.9	−1.08
1	12	207.4	7.34	245	796.5	98.4	2.02	38.01	0.44
0.251	12.5	363.7	5.57	175	1396.5	172.5	2.42	40.67	−1.16
1	12.5	211.4	4.42	26	811.9	100.2	2.01	40.24	0.41

Table 3
Comparison of unit size, CAPEX, EnEx, and water recovery between laboratory-scale operational conditions (experimental soda concentration) and simulated pilot-scale operational conditions (1 M soda) in the scenario involving NF retentate as feed stream.

OH- Conc [M]	pH	NF [m^2]	Reactor [L]	Soft. resin [m^3]	EDBM [Triplet]	MD [m^2]	RED [m^2]	CAPEX [M€]	EnEx [kW]	Water Rec [m^3]
0.31	10.6	63.2	202.7	9.05	139	871.3	107.5	2.01	34.03	−0.60
1	10.6	63.2	121.1	9.03	188	557.9	68.8	1.78	32.24	0.24
0.437	12.5	61.0	199.3	6.55	222	854.7	105.6	2.08	39.18	−0.56
1	12.5	61.0	132.6	6.42	267	598.5	73.8	1.87	39.33	0.09

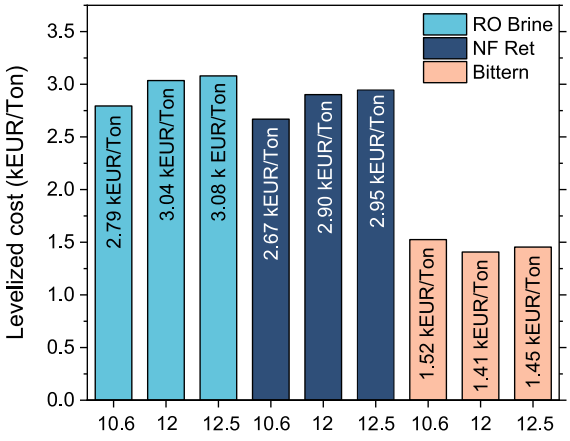

Fig. 10. Levelized cost of $Mg(OH)_2$ for the RO brine, NF retentate, and bittern scenarios at different pH values. RO brine yields the highest costs due to large flowrates, NF retentate shows intermediate costs, and bittern yields the lowest, though negative water balances reduce circularity.

of 1450 €/ton, 1320 €/ton, and 1370 €/ton, were obtained for the three pH values investigates, values closer to the market value of 1000 €/ton. Results agree with those reported by Scelfo et al. [42] for the case of the SEArcularMINE treatment chain. Specifically, a techno-economic analysis conducted at pilot-scale targeting 50 tons/year of $Mg(OH)_2$ treating RO brine, NF retentate and saltworks bitterns led to values of 3.14, 2.66, and 1.58 €/kg$Mg(OH)_2$ [42]. In this latter case, the authors also considered slurry treatment units such as a thickener, a washer and a drum filter in their analysis.

Values decreased of about 70 % in an industrial scale-up scenario (from 50 tons/year to 5000 tons/year) [42]. Therefore, considering a similar reduction factor, $Mg(OH)_2$ levelized costs between 0.5 and 0.9 €/kg$Mg(OH)_2$ might be achieved in the CARMEn chain, thereby making this process economically attractive for the production and commercialization of magnesium hydroxide.

4. Conclusions

In the present work, the technical and economic feasibility of the novel circular brine treatment chain presented by the CARMEn project was assessed. The treatment chain aimed at valorizing waste saline solutions from desalination plants and saltworks to recover magnesium hydroxide, $Mg(OH)_2$. An extensive laboratory-scale experimental campaign was performed as proof of concept, and based on the experimental data, a preliminary techno-economic analysis was conducted at pilot scale targeting a production capacity of 50 ton/year of magnesium hydroxide under three reaction pH conditions (10.6, 12, and 12.5). Three saline solutions were analyzed as feed stream: (i) RO brine, (ii) NF retentate, that is, the retentate stream from an NF unit fed with the RO brine, (iii) saltworks bittern.

The use of the RO brine showed the highest CAPEX and EnEx due to the large solution volumes treated in the chain. Increasing the reaction pH raised both CAPEX and EnEx, as higher NaOH production volumes were required from the EDBM unit. For the NF retentate, the CAPEX of the reactor decreased owing to the higher Mg^{2+} concentration in the solution, although the additional cost of the NF unit had to be included. The use of the bittern, whose Mg^{2+} concentration was 20 times higher than that of the RO brine, halved both CAPEX and EnEx. However, this scenario resulted in a negative net water balance, requiring an external water input approximately 5–6 times that of the feed saline solution. By contrast, the use of RO brine and NF retentate did not require any external water input. Importantly, the use of bittern enabled the production of highly pure $Mg(OH)_2$ solids (purity >99.7 %), thanks to its low Ca^{2+} content.

The levelized cost of $Mg(OH)_2$ from bittern was found to be almost half that calculated for RO brine and NF retentate scenarios, though still roughly 45 % above current market price of 1000 €/ton. Coupling the MD unit with waste heat significantly reduced costs, achieving a minimum $LC_{Mg(OH)_2}$ value of 1320 €/ton for bittern processed at pH 12. It is important to highlight that levelized cost of $Mg(OH)_2$ are expected to at least halve in industrial scale-up scenarios, thus marking the economic viability of the proposed chain.

As take-home messages, for a treatment chain to produce $Mg(OH)_2$ compounds from Mg^{2+} containing solutions:

- Concentrated Mg^{2+} and NaOH solutions, can reduce CAPEX by reducing processed volumes, with a less influence on EnEX.
- The reaction pH strongly affects several parameters. Higher pH increases EDBM CAPEX/EnEx (more NaOH required), but decreases softener CAPEX (greater divalent removal in the reactor), while reducing product purity in Ca^{2+} containing solutions due to co-precipitation.
- The use of Ca-free solutions, such as saltworks bitterns, can lead to the production of highly pure $Mg(OH)_2$ solids (>99.7 %), but may require external water input, compromising process circularity.
- The coupling of the MD unit with waste heat sources can drastically reduce the energy requirement of the chain.

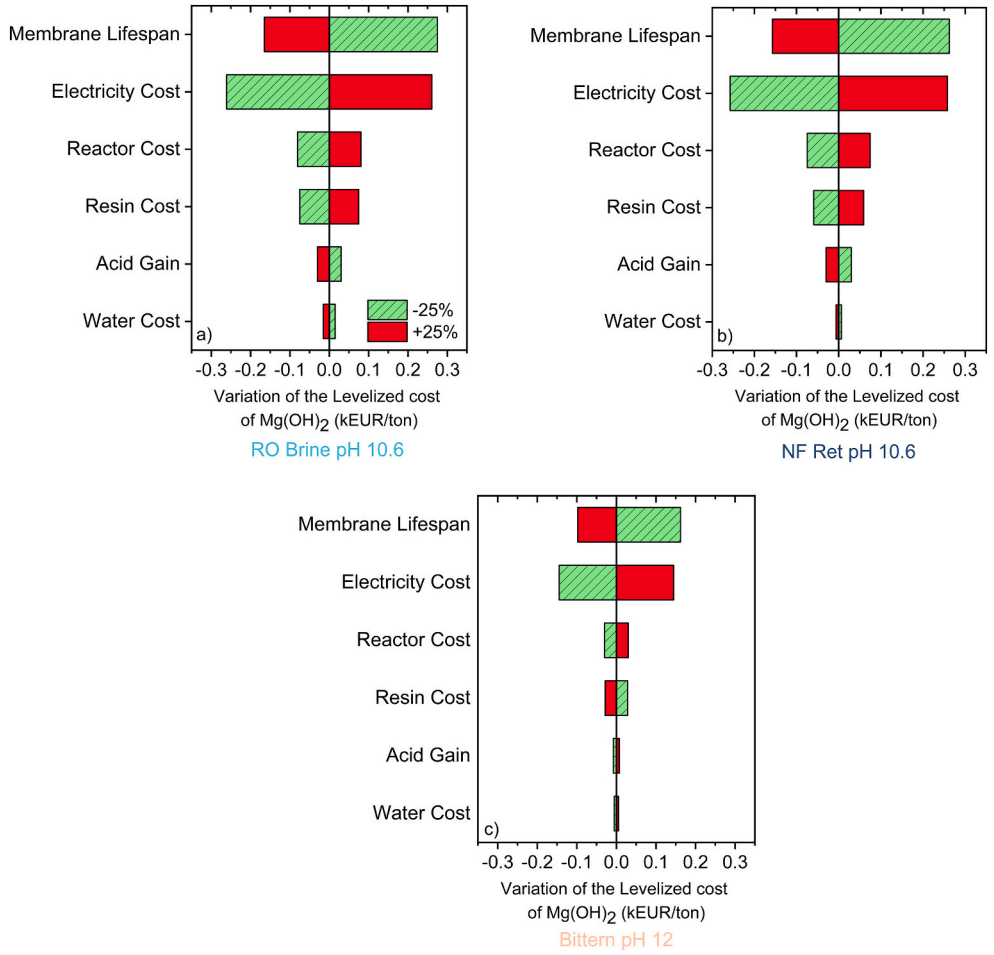

Fig. 11. Variation of the Levelized cost of $Mg(OH)_2$ (euro) as a function of (i) water cost, (ii) acid cost, (iii) resin cost, (iv) reactor cost, (v) electricity cost, (vi) membrane lifespan by a factor of 25 %, for the case of (a) RO brine at pH 10.6, (b) NF ret. at pH 10.6 and (c) Bittern at pH 12.

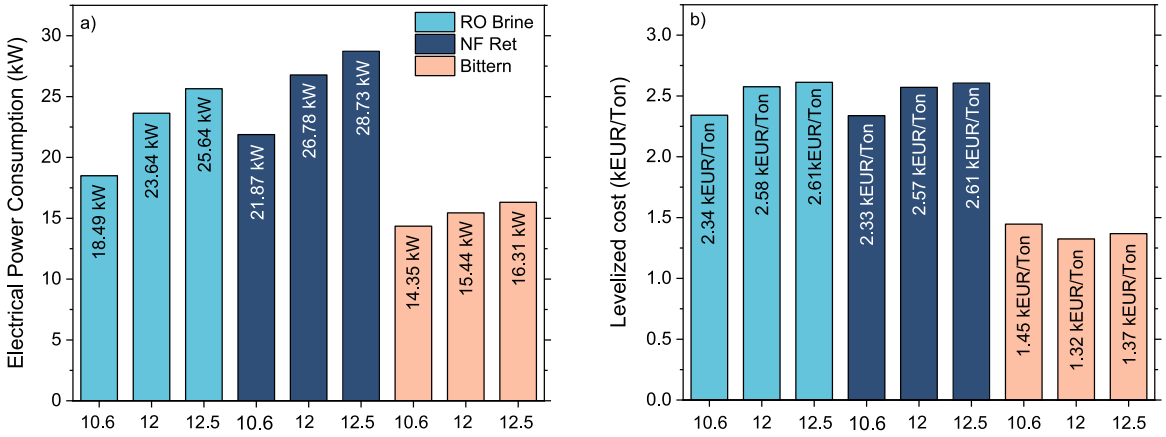

Fig. 12. Effect of waste heat integration on electrical power consumption (left) and levelized cost of $Mg(OH)_2$ (right). Waste heat reduces electrical demand by ~30 % for RO brine and NF retentate cases, with smaller reductions for bittern. Levelized cost of $Mg(OH)_2$ decreases but remains above market values at pilot scale.

Overall, the techno-economic analysis, validated by the experimental campaign, showed that circular approaches can represent reliable solutions for the sustainable production of high added value compounds from waste. Operational parameters (such as NaOH concentration), feed composition, process design, and energy integration strategies critically influence the trade-offs between economics, circularity, and product quality, emphasizing that technological optimization combined with energy integration is key to unlocking the circular economy potential of saline waste valorization. It is also worth noting that many of the technologies of the CARMEn project are still at demonstration scale, with research activities devoted to their industrial scale-up and application. Dedicated long-run tests should be performed in order to assess issues of module fouling and membrane properties deterioration, as well as a Life Cycle Assessment of the chain to measure its environmental benefits and trade-offs.

Nomenclature

AGMD	Air-gap membrane distillation
CAPEX	Capital expenditure
CE	Current efficiency
DCMD	Direct contact membrane distillation
EDBM	Electrodialysis with bipolar membrane
EnEx	Energetical expenditure
LC	Levelized cost
MD	Membrane distillation
MED	Multiple effect distillation
MVC	Mechanical vapor compression
NF	Nano filtration
OCV	Open Circuit Voltage
RED	Reverse electrodialysis
RO	Reverse osmosis
TDS	Total dissolved salts
V-AGMD	Vacuum – air-gap membrane distillation

CRediT authorship contribution statement

Giuseppe Scelfo: Writing – original draft, Visualization, Software, Methodology, Investigation, Formal analysis, Data curation. **Giuseppe Battaglia:** Writing – review & editing, Visualization, Validation, Supervision, Methodology, Investigation, Formal analysis, Data curation, Conceptualization. **Michela Cardella:** Visualization, Validation, Investigation, Formal analysis. **Antonella Filingeri:** Visualization, Validation, Investigation, Formal analysis. **Andrea Culcasi:** Visualization, Validation, Investigation, Formal analysis. **Francesco Volpe:** Visualization, Validation, Investigation, Formal analysis. **Lorenzo Craveri:** Visualization, Validation, Investigation, Formal analysis. **Erica Bertozzi:** Visualization, Validation, Investigation, Formal analysis. **Alberto Tiraferri:** Writing – review & editing, Supervision, Resources, Project administration, Methodology, Conceptualization. **Giorgio Micale:** Supervision, Resources, Project administration, Methodology, Conceptualization.

Declaration of competing interest

The authors declare that they have no known competing financial interests or personal relationships that could have appeared to influence the work reported in this paper.

Acknowledgments

This work was supported by the Made in Italy Circolare e Sostenibile (MICS) Extended Partnership (PNRR Project No. PE_00000004) funded by the European Union NextGenerationEU.

Appendix A

A.1. The Carmen treatment chain

Laboratory-scale testing of the chain was conducted as a proof of concept to demonstrate the feasibility and effective implementation of the proposed concept. To this aim, two feed solutions were examined: (i) 30 L of Reverse Osmosis (RO) brine from the industrial desalination plant of Lampedusa Island and (ii) 30 L of bittern from Trapani saltworks. The ion composition of two solutions is provided in Table A1. Ion concentration was measured through IC analysis (IC, 930 Compact IC plus, Metrohm), while the content of bicarbonates was obtained from the total alkalinity of the solution measured through titration with sulfuric acid (Honeywell-Fluka, 95–97 % w/w), according to the APAT 2010 method (see also ISO 9963-1).

Table A1
Ion composition in mg/L of real RO brine and bittern solutions.

	RO brine	Bittern
Na^+	18,000	55,000
K^+	600	13,000
Ca^{2+}	750	165
Mg^{2+}	2000	49,000
Cl^-	32,350	192,100
SO_4^{2-}	4000	61,000
Br^-	140	2100
HCO_3^-	220	1460

A.2. Experimental set-ups and procedures

A.2.1. Nanofiltration (NF) unit

Nanofiltration tests were performed using a bench-scale cross-flow system made of (i) a 30 L feed tank, (ii) a high-pressure pump (Hydra-cell pump, Wanner Engineering, Inc., USA), and (iii) a membrane module (model Sepa, Sterlitech, USA) that hosted a flat-sheet membrane with a total active area of 140 cm^2, see Fig. A1. A back-pressure valve (Swagelok, USA) was used to set the desired pressure in the system. Pressure and flow rate values were monitored by using a manometer (SPAN, USA) and a flowmeter (model 1900 ASA, Italy). Temperature was regulated through a recirculating chiller (model MC 1200, Lauda, Germany) equipped with a stainless-steel coil submerged in the feed tank. The system was operated in an open-loop mode at a cross-flow velocity of 0.23 ± 0.02 m/s; a feed hydraulic pressure of 68 ± 4 bar; and feed solution temperature of 22.5 ± 2.5 °C. Feed water exiting the housing cell was directly recirculated into the feed tank, while the permeate was collected in a tank placed on a computer-interfaced scale, allowing for continuous measurement of the permeate flux.

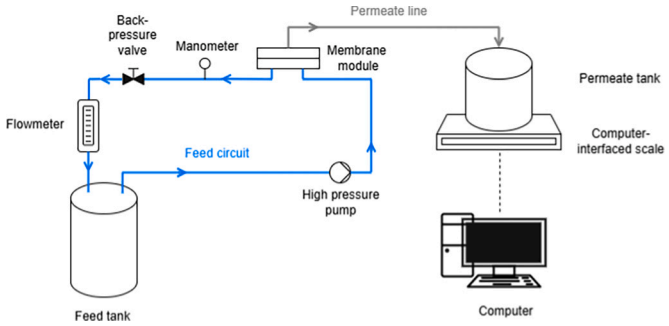

Fig. A1. Scheme of the bench-scale cross-flow system used for the NF tests.

The salt rejection performance of the NF unit was evaluated in term of observed rejection ($R_{observed}$), which was calculated as follows:

$$R_{observed}(\%) = \left(1 - \frac{C_p}{C_f}\right) \cdot 100 \quad \text{(A.1)}$$

where C_p and C_f are the concentration of salt in permeate and feed streams, respectively, evaluated by measuring the electrical conductivity of the two streams with a conductivity meter (XS COND 70 VIO, XS instruments, Italy). This equation is similar to Eq. (3).

The recovery rate of the unit, here evaluated as the ratio between the collected permeate volume, V_p (L), and the initial feed volume, V_f (L), was calculated as follows:

$$Rec_{NF}\ (\%) = \frac{V_p}{V_f} \cdot 100 \quad \text{(A.2)}$$

Tests were conducted using different membranes. Specifically, the NFW (TFC 300-500 Da) from Synder Filtration (Vacaville, CA, USA) was selected to process the RO brine, while a NF270 membrane from DuPont was selected for the bittern. Table A2 reports the main characteristics of the tested membranes.

Table A2
Characteristics of the adopted membranes as provided by the manufacturer.

	Nominal molecular weight cut-off	Nominal NaCl rejection	Nominal $MgSO_4$ rejection
NFW[a]	300–500 Da	20.0 %	97 %
NF 270[b]	Not provided	n.a.	~97 %

[a] Salt rejection of 200 ppm of salt, 7.6 bar operating pressure, 25 °C, unknown recovery.
[b] Salt rejection of 2000 ppm of salt, 4.8 bar operating pressure, 25 °C, 15 % recovery.

A.2.2. $Mg(OH)_2$ recovery

$Mg(OH)_2$ tests were carried out in a laboratory scale continuous stirred reactor (CSTR) made of: (i) a 1 L plexiglass reactor, (ii) a Rushton six-blade turbine and (iii) pumps (Kronos 50) for solutions handling, as shown in Fig. A2. Experiments were carried out aiming at determining the best operating conditions to produce highly pure $Mg(OH)_2$ powders treating (i) the RO brine, (ii) the NF retentate solution, i.e., the bivalent concentrated solution outcoming the NF unit, and (iii) the bittern.

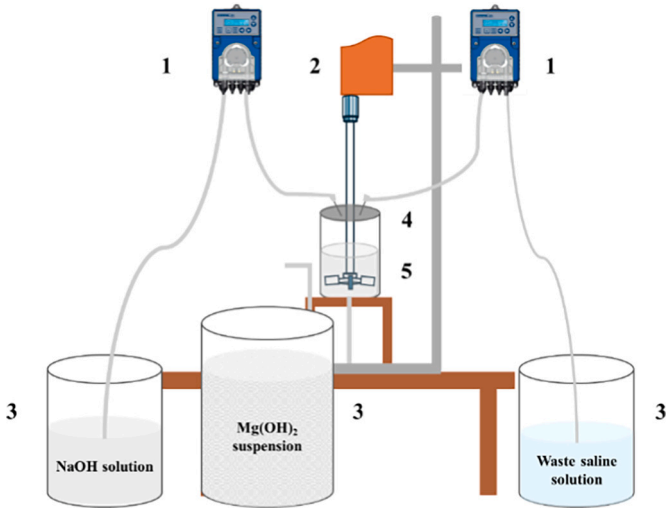

Fig. A2. Schematic representation of the CSTR laboratory set-up employed from $Mg(OH)_2$ precipitation tests: (1) peristaltic pumps (Kronos, 50), (2) a stirrer motor (LLG LABWARE), (3) containers for feed and product solutions; (4) reactor; (5) Rushton turbine.

Saline and alkaline solutions were pumped into the reactor that was filled with 750 mL of demi water at the beginning of each test. The suspension

was stirred at 400 rpm. Synthetic NaOH solutions were used as alkaline reagent and prepared by dissolving NaOH flakes (Inovyn, purity grade > 99 %, technical grade) in demi-water. The concentration of the magnesium and calcium ions was measured by complexometric titration with ethylenediaminetetraacetic acid (EDTA), while the concentration of NaOH solutions was measured via acid-base titration. The pH of the synthesized suspensions was measured in the outlet tank using a portable pH-meter (WTW 8830). Three final pH values were investigated: (i) a slightly higher stoichiometric reaction pH value, 10.6 [69] and two hydroxide ions excess conditions, i.e. (ii) pH of 12.0 and (iii) 12.5. In the case of the NF retentate solution, due to the limited amount of the solution, only pH values of 10.6 and 12.5 were analyzed.

Table A3 reports the operating conditions for all tests, Mg^{2+} and Ca^{2+} concentration in the saline solutions along with that of hydroxyl ions in the NaOH solutions.

Table A3
Saline and NaOH solution concentrations, operating conditions for $Mg(OH)_2$ tests.

	RO brine pH 10.6	RO brine pH 12.0	RO brine pH 12.5	NF ret pH 10.6	NF ret pH 12.5	Bittern pH 10.6	Bittern pH 12.0	Bittern pH 12.5
Mg^{2+} [mol/L]	0.086	0.086	0.086	0.155	0.155	0.980	0.980	0.980
Ca^{2+} [mol/L]	0.018	0.018	0.018	0.027	0.027	0.002	0.002	0.002
OH^- [mol/L]	0.172	0.21	0.251	0.31	0.437	1.000	1.000	1.000
Brine flowrate [mL/min]	40	40	40	40	40	40	40	40
NaOH flowrate [mL/min]	40	40	40	40	40	40	89.6	104
Final pH	10.6	12.0	12.5	10.6	12.5	10.6	12.0	12.5

After precipitation, $Mg(OH)_2$ suspensions were let to settle and clarified solution collected for analysis. Mg^{2+} and Ca^{2+} concentrations were measured by EDTA. From concentrations, the recovery of magnesium (Rec_{Mg}) and calcium (Rec_{Ca}) ions were estimated by following Eq. (A.3):

$$Rec_i = \frac{C_i^{in} Q_S - C_i^{fin}(Q_S + Q_{alk})}{C_i^{in} Q_S} \tag{A.3}$$

where C_i^{in} and C_i^{fin} are the concentrations (mol/L) of magnesium (Mg^{2+}) or calcium (Ca^{2+}) ions in the saline solutions and in the clarified ones, respectively; Q_S and Q_{alk} are the flow rates (mL/min) of the saline and NaOH solutions, respectively. Thickened $Mg(OH)_2$ suspensions were washed with demi-water until the conductivity of the supernatant solution was <200 μS/cm. Washed $Mg(OH)_2$ suspensions were then filtered and dried in oven at 120 °C for about 24 h. The dried cake was milled and crystalline structure analyzed by X-ray diffraction, XRD, technique using CuKa radiation (1.542°A, 40 KV, 100 mA) in the 2θ range of 10–70° at a step size of 1°/min by using the RIGAKU model D.MAX 2500 HK. Purity of solids was also assessed by dissolving ~150 mg in ultrapure hydrochloric acid (HoneywellFluka;>30 % for trace analysis) and liquids analyzed through ion chromatography (IC) (Metrohm model 882 compact IC plus). The cationic purity was then calculated as:

$$Cationic\ purity = \frac{C_{Mg2+}}{\sum_{i=1}^{N} C_i} \tag{A.4}$$

where C_{Mg2+} and C_i are the concentration of Mg^{2+} and *i-th* cation detected by the IC.

A.2.3. Electrodialysis with bipolar membrane unit (EDBM)

Clarified saline solutions of $Mg(OH)_2$ tests were first pre-treated to remove any remaining traces of calcium and magnesium ions in excess of 10 ppm of equivalent $CaCO_3$, which is the maximum limit allowed for EDBM application [38]. An ion exchange resin (Purolite™ S940) was employed to remove Mg^{2+} and Ca^{2+}. Solutions were pumped at 12 mL/min through a Kronos 50 peristaltic pump, see Fig. A3a. The Mg^{2+} and Ca^{2+} content in the clarified saline solution before and after the pre-treatment step was determined by complexometric titration (EDTA) and were reported in Table A4.

Table A4
Total hardness, i.e., the sum of the content of Ca^{2+} and Mg^{2+}, of tested clarified solutions before and after the treatment with ion exchange resins.

	RO brine			NF retentate		Bittern		
Total hardness [ppm]	pH 10.6	pH 12.0	pH 12.5	pH 10.6	pH 12.5	pH 10.6	pH 12.0	pH 12.5
Before ion exchange resin	340	216	80	552	108	416	0	0
After ion exchange resin	0	1.2	1.2	0	0	0.8	0	0

EDBM tests were carried out in batch (closed-loop) mode with a laboratory-scale EDBM unit (Electromat MkI ED STACK, supplied by WTS) equipped with five membrane triplets, each with an active area of 0.028 m^2. The experimental set-up of the EDBM unit is shown in Fig. A3b.

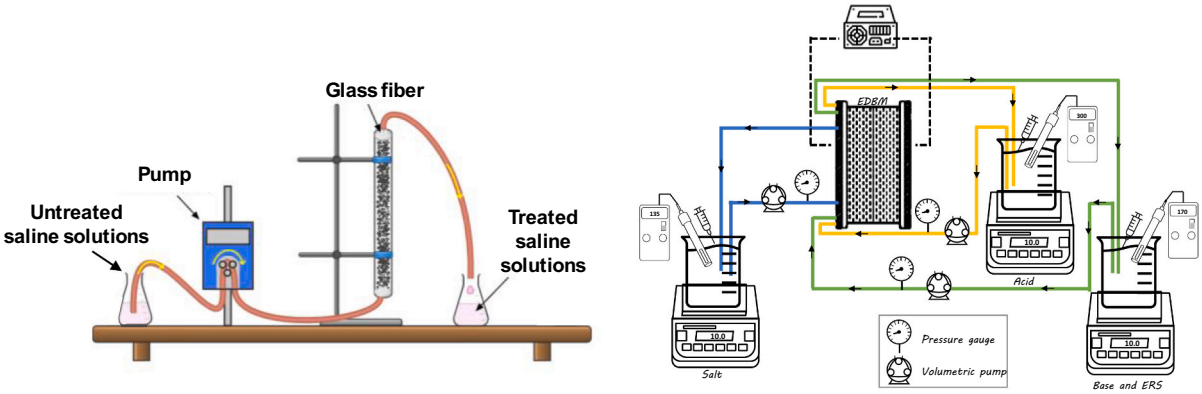

Fig. A3. Schematic representations of a) ion-exchange resin experimental setup to remove calcium and magnesium ions and b) the EDBM experimental setup.

Peristaltic pumps (YT15, BT601S Lead Fluid, CO LTD, China) were employed to feed the solution into the stack. Each triplet of the EDBM unit comprised a cation-exchange membrane (CR61N), an anion-exchange membrane (AR103N) and a bipolar membrane. Specifically, the bipolar membrane used consists of two layers: the cationic layer is a CR61N Cation Exchange Membrane (CEM), while the anionic layer is an AR103N Anionic Exchange Membrane (AEM), treated by the manufacturer to incorporate a catalyst that promotes the water dissociation reaction. Properties of membranes were reported in Table A5.

Table A5
Properties of cation (CEM) and anion (AEM) exchange membranes used in this work [70].

Membrane	Name	Wet membrane thickness [μm]	Areal resistance[a] [Ω cm^2]	Permselectivity [%]	IEC[b] [meq/g]	Burst strength [psi]
CEM	CR61N	300	3.6	95	2.20	95
AEM	AR103N	300	2.8	95	2.37	95
AEM-treated	AR103N-tr.	n.a.	n.a	n.a	10.6	n.a

[a] Measured in 0.1 mol/L NaCl solution.
[b] IEC refers to meq/dry g of resin.

Polystyrene spacers were interposed between the membranes to form the acid, base and salt solution channels. These spacers were 760 μm thick and had an S-shape design to promote solution mixing and avoid dead zones. Two additional overlapped spacers were used to form the Electrode Rinse Solution (ERS) channels located on both sides of the EDBM stack. Flat plates made of stainless steel and stainless steel with a platinum coating were used as the electrodes. Platinum wires (99.9 % metal basis, 127 μm of diameter, Alfa Aesar) were placed: i) between the anode and its nearest CEM, and ii) between the cathode and its nearest CEM. These Pt-wires were included to monitor the effective voltage applied to the 5 triplets, thereby excluding the electric potential applied to the electrodic chambers. The pre-treated brine solution (without Mg^{2+} and Ca^{2+}) were fed into the salt channel, with a fixed initial volume solution of the acid and base to match the required volume of base to be adopted in the $Mg(OH)_2$ tests. The initial acid and base solutions (concentrations equal to 0.05 mol/L) were prepared using a concentrated HCl solution (ACS Reagent 37 %, Honeywell, Fluka) and solid sodium hydroxide micro pearls (technical grade, Inovyn), respectively. The same alkaline solution circulating in the base compartments also feeds the ERS compartments (i.e., anodic and cathodic). Since the process operated in batch mode, the concentration of the alkaline solution—and consequently that of the ERS—increased over time. However, this did not significantly affect the electrodic reactions. Furthermore, for each mole of hydroxyl ion consumed at the anode during oxygen evolution, an equivalent amount is produced at the cathode during hydrogen evolution. As a result, there was no net change in OH^- concentration due to the electrodic reactions.

Table A6 presents the initial volumes of saline, alkaline and acidic solutions utilized in each EDBM test.

Table A6
Initial volume of saline, alkaline and acidic solutions fed in the EDBM unit.

	RO brine pH 10.6	RO brine pH 12	RO brine pH 12.5	NF retentate pH 10.6	NF retentate pH 12.5	Bittern pH 10.6	Bittern pH 12.0	Bittern pH 12.5
Saline volume	3.50 L	4.00 L	3.20 L	3.80 L	3.75 L	2.50 L	3.75 L	3.25 L
Alkaline volume	4.50 L	4.50 L	4.50 L	4.50 L	4.50 L	1.25 L	1.90 L	1.60 L
Acid volume	4.50 L	4.50 L	4.50 L	4.50 L	4.50 L	2.50 L	3.75 L	3.25 L

After assembling the stack, internal and external leakage tests were carried out by feeding deionized water into the three compartments without applying any electric current. No external leakage was observed, and only negligible internal leakage (below 5 %) was measured. These leakage tests were periodically performed during the experimental campaign. Before starting each EDBM experiment, the saline, acid and alkaline solutions were recirculated into the empty stack, and air was removed from the stack and the piping. The Open Circuit Voltage (OCV) was measured before applying the operating current density at 200 A/m^2. The flowrates of the solutions were fixed in order to maintain a mean channel flow velocity of around 7 cm/s, as suggested by the manufacturer. A power supply (1902B, B&K precision) was connected to the EDBM stack to apply the electric field. The voltages of the stack and platinum wires were measured utilizing a portable multimeter (Fluke 175). An additional portable multimeter was connected in series to verify the current intensity measurement. Samples of 5 mL were taken from each tank during each test with a syringe. Solution mass, electrical conductivity, pH and temperature were monitored over time using precision scales (KERN KB, Max 10,000 g, d = 0.1 g) and a portable pH and conductivity meter (WTW 314). Tests were stopped when the alkaline solution reached the target operating OH^- concentration. Samples were periodically collected during the tests and subsequently analyzed by titration to determine the concentration of H^+ and OH^-. Specifically, standard solutions of 0.1 mol/L HCl, 0.05 mol/L Na_2CO_3 were used to carry out base and acid titrations, respectively. A 0.1 % Methyl Orange solution (ACS dye content 85 % *w*/w, SIGMA-ALDRICH) was adopted as visual pH indicator for both titrations.

The performance of the EDBM process were evaluated using performance indicators such as the Specific Energy Consumption (*SEC*) and the Current Efficiency (*CE*). Both parameters were related to the alkaline solution, as the NaOH is the main product of the EDBM unit and has the larger economic value.

The *SEC* (kWh/kg_{NaOH}) measures the energy required to produce 1 kg of NaOH and it was defined as:

$$SEC = \frac{I \cdot \int_0^t V_{Pt} \cdot dt}{3,600 \cdot \left(V_{NaOH,t} \cdot C_{NaOH,t} - V_{NaOH,0} \cdot C_{NaOH,0}\right) \cdot M_{NaOH}} \tag{A.5}$$

where I (A) and V_{Pt} (V) are the constant applied electric current and the measured voltage at platinum wires, respectively; t (s) is the process time; V_{NaOH} (L) and C_{NaOH} (mol/L) are the NaOH solution volume and concentration, respectively; M_{NaOH} (g/mol) is the NaOH mole mass. The subscripts t and 0 refer to the generic time t and to the beginning of the test, respectively. Volume values were calculated from the solution masses, which were measured using scales.

OH^- current efficiency, *CE* (%), is the fraction of the applied electric current that is converted into OH^- ions generated at the bipolar membrane interlayer, this was defined as:

$$CE = \frac{\left(V_{NaOH,t} \cdot C_{NaOH,t} - V_{NaOH,0} \cdot C_{NaOH,0}\right) \cdot z\, F}{I \cdot N \cdot t} \cdot 100 \tag{A.6}$$

where z is the ion valence, F is the Faraday Constant (equal to 96,485C/mol), and N represents the number of triplets.

A.2.4. Membrane distillation unit (MD)

A direct contact MD system, i.e., both feed and distillate solution in contact with a polyethylene membrane (Aquastill, Netherlands), was adopted for solution concentration and fresh water reclamation. The setup, see Fig. A4, included a feed tank, a distillate tank, two gear pumps (one for each stream, Fluid-o-Tech, Italy), and a two-plate cell module for membrane housing. The flow rate of both solutions was 25 L/h controlled by two flowmeters (ASA, Italy). Feed and permeate (or distillate) solutions were fed at 45 °C and 20 °C, respectively. Temperature was controlled with a heater (Thermo Fisher, USA) and a cooler (Ametek Brookfield, USA). The electrical conductivity of permeate and feed solution was continuously measured with a XS COND 70 VIO conductivity meter (XS instruments, Italy).

The NF retentate solution (around 2.5 L) was tested in a 10 cm wide and 14 cm long module (Sepa Acrylic, Sterlitech, USA), resulting in a total membrane active area of 140 cm^2. In contrast, the RO brine (around 7.7 L) and bittern (7 L) solutions were fed into a larger stack (Aquastill, Netherlands), measuring 10 cm in width and 54 cm in length, and resulting in a total active area of 540 cm^2. For each saline solution category, the outcoming saline solutions from the EDBM at different pH values were mixed and treated together. The distillate tank was initially filled with approximately 1.2 L of deionized water.

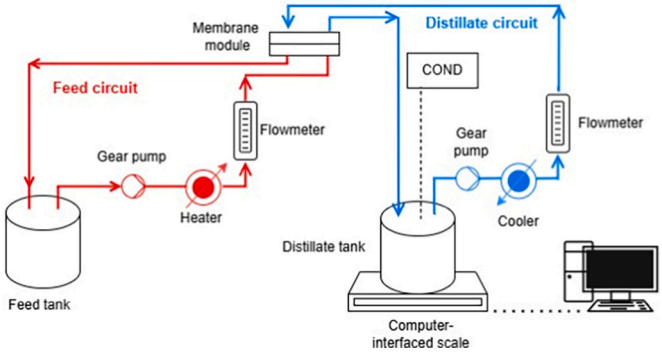

Fig. A4. MD experimental setup. In red, the feed circuit; in blue, the permeate/distillate circuit. The two solutions meet in the two plate module containing the membrane, and then return to their respective tank. Electrical conductivity of the permeate was monitored using probes directly immersed in the tank, while flux data were collected monitoring the change in weight of the permeate tank by means of a computer-interfaced scale.

Tests were conducted aiming at a final feed solution electric conductivity value of ~150–160 mS/cm.

During MD tests, the concentration (in terms of electrical conductivity) of permeate solution, C_d, was evaluated using Eq. (A.7):

$$C_d = \frac{V_i C_i - V_{i-1} C_{i-1}}{V_d} \tag{A.7}$$

where V_i and C_i are the volume and the conductivity of the solution in the permeate tank at the *i-th* time, while V_{i-1} and C_{i-1} are those at the previous *i-th* instant. V_d indicates the volume of permeate collected between the *i-1* and the *i* time. The rejection was calculated as follows:

$$R_{MD}(\%) = \left(1 - \frac{C_d}{C_f}\right) \cdot 100 \tag{A.8}$$

where C_f is the conductivity of the feed solution. The recovery rate, the ratio between the collected permeate volume (V_p) and the initial feed volume (V_f) was calculated as follows:

$$Rec_{MD}\ (\%) = \frac{V_p}{V_f} \cdot 100 \tag{A.9}$$

A.2.5. Reverse electrodialysis unit (RED)

RED tests were carried out in a laboratory-scale unit (REDstack B.V., The Netherlands) equipped with three cell pairs with an active area of 0.01 m^2 (0.1 m × 0.1 m) each. The cell pair was composed of either cation or anion-exchange Fujifilm Type 10 membranes, specifics of the membranes can be found in Moreno et al. [71]. Polyethersulfone (PES) 270 μm thick woven spacers (Deukum GmbH, Germany) were placed between membranes to create high and low salinity solution channels. A silicon gasket and an additional woven spacer were used to assemble each of the two ERS channels, positioned at both ends of the RED unit. Anode and cathode electrodes were of Ru—Ir oxides coated titanium materials. The electrode rinse solution was a mixture of 0.2 mol/L $K_4Fe(CN)_6 \cdot 3H_2O$ (99 % purity ChemSolute®, Germany), 0.2 mol/L $K_3Fe(CN)_6$ (99 % purity ChemSolute®, Germany) and 1.0 mol/L NaCl (99.5 % purity Carlo Erba Reagents, Italy), which was recirculated in electrodes compartments at a flowrate of 150 mL/min. Three peristaltic pumps (Lead Fluid YT15) were adopted for the hydraulic circuits of ERS, high and low salinity solutions. A schematic representation of the experimental apparatus is reported in Fig. A5.

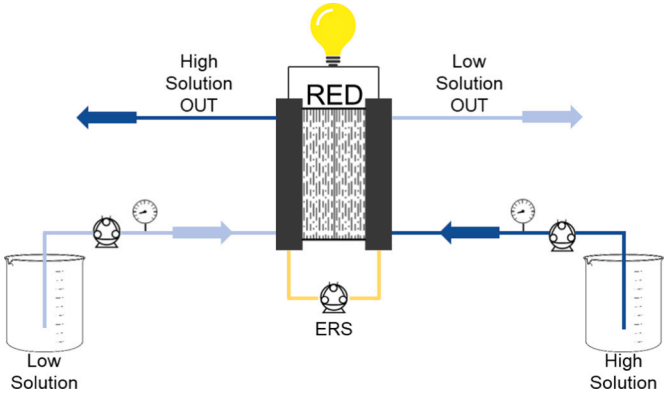

Fig. A5. Schematic representation of RED lab-scale set-up.

RED tests were conducted in open-loop configurations and solutions were pumped in a co-current flow configuration. Leakage tests were performed as for EDBM units, observing negligible internal leakage. Before each test, air bubbles were removed from the stack and the hydraulic circuits. In all tests, the flow velocity of the high and low salinity solutions was 0.5 cm/s and 1.0 cm/s, respectively. A real reclaimed water from an industrial transformation of citrus, adequately treated before the use [72,73] with an electrical conductivity of 1.5 mS/cm, was the low saline solution.

The OCV was measured in each test before connecting an external load in series to the stack. During the tests, the stack voltage, E_{stack} (V), and current, I (A), were measured, at variable external loads connected, through portable multimeters (Fluke 175). Values were used to quantify the power output of the stack. Pressure drops were measured via two pressure gauges (Cewal S.p.a., Italy) and then used to calculate energy consumption and power loss. RED performance was then evaluated referring to gross, $P_{d,gross}$, and net power, $P_{d,net}$, density (W/m^2), calculated as:

$$P_{d,gross} = \frac{E_{Stack} I}{N \cdot A} \tag{A.10}$$

$$P_{d,net} = P_{d,gross} - \frac{Q_H \Delta p_H + Q_L \Delta p_L}{N \cdot A} \quad (A.11)$$

where Δp_H and Δp_L are the measured pressure drops (Pa) between the inlet and outlet of high (H) and low (L) salinity ~ compartments (Pa), Q_H and Q_L are the solutions flow rates (m^3/s), N is the number of cell pairs and A is the active membrane area of a cell pair (m^2).

The performance of a RED unit depends also on the resistance of the electrode compartment, R_{blank}, which can have a massive impact in unit assembled with a small number of cell pairs. R_{blank} was measured following the experimental procedure reported in literature [74], reporting a value of 0.247 Ω.

Table A7 reports composition and electric conductivity of high and low salinity solutions. Ionic composition was assessed using a Metrohm 882 compact IC plus Ion Chromatograph equipped with a Metrosep A Supp 5 – 250/4.0 anion column, for anions, and a Metrohm 930 compact IC plus Ion Chromatograph equipped with a Metrosep C 4 – 250/4.0 cation column, for cations. The high saline solutions were the outlet concentrated solutions of the MD unit.

Table A7
Ion composition of high and low salinity solutions measured by Ion chromatography. Conductivity values were also reported.

	Bittern	RO brine	NF retentate	Reclaimed water
Na^+ [mol/L]	2.37	1.65	2.35	0.004
K^+ [mol/L]	0.07	0.015	0.015	0.005
SO_4^{2-} [mol/L]	0.44	0.10	0.21	0.002
Cl^- [mol/L]	1.23	1.37	1.92	0.005
Conductivity [mS/cm]	155.5	129.3	155.7	1.5

A.3. Results and discussion

A.3.1. Nanofiltration

Fig. A6 shows the permeate flux and the observed rejection, Eq. (A.1), as a function of recovery rate, Eq. (A.2), for NF tests carried out feeding RO brine using the Synder NFW membrane.

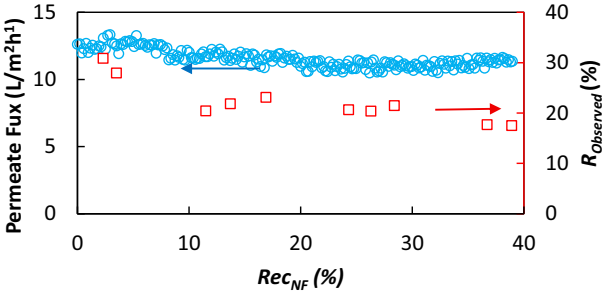

Fig. A6. NF tests treating the RO brine solution: water flux (left axis, blue circles) and observed rejection (%), Eq. (A.1), (right axis, red squares) as function of the recovery rate (%), (Eq. (A.2), bottom axis).

Tests lasted ~72 h. The water flux (blue circles in Fig. A6) showed a marginal decline over the course of the experiment, decreasing from an initial value of about 12.6 L/m^2h^1 to values of about 11–11.5 L/m^2h^1 at a recovery rate of 20 %. Thereafter, the flux remained largely constant for the rest of the test. This behavior was expected due to fouling and scaling phenomena [75], as well as for the progressive concentration of the feed solution [76,77]. The observed rejection declined monotonically from an initial value of 30.9 % to a final one of 17.5 %. This trend was somewhat expected, as the gradual concentration of the feed solution reduces membrane rejection [78,79]. Nonetheless, results were in adequate agreement with the membrane characteristics provided by the membrane manufacturer. The pH of the feed solution did not vary during experiments, being ~6.5 over time. After the test, HCl was used to lower the pH to 5, preventing possible metal precipitation before sample analysis.

As far as the bittern solution is concerned, the high concentration of ions in the bittern significantly compromised the process. In fact, the water flux was ~0.3 $L\,m^{-2}\,h^{-1}$ and $R_{observed}$ was ~2 %. In fact, due to the extremely high salinity of the solution, often exceeding 6 M (total salinity), it is necessary to overcome an osmotic pressure of more than 100–150 bar to obtain a not negligible water flux. This makes the process highly challenging and energy-intensive, primarily due to the high pressures required. Furthermore, it is nearly unfeasible with conventional membranes, which are not designed to withstand such elevated operating pressures. No commercially available nanofiltration membrane is expected to provide feasible performance in terms of flux and ion separation.

A.3.2. $Mg(OH)_2$ recovery unit

Fig. A7 reports Mg^{2+} and Ca^{2+} recoveries. Eq. (A.3) evaluated for all tests. The precipitation of calcium compounds was not desired as it affects the purity of the synthesized $Mg(OH)_2$ powders.

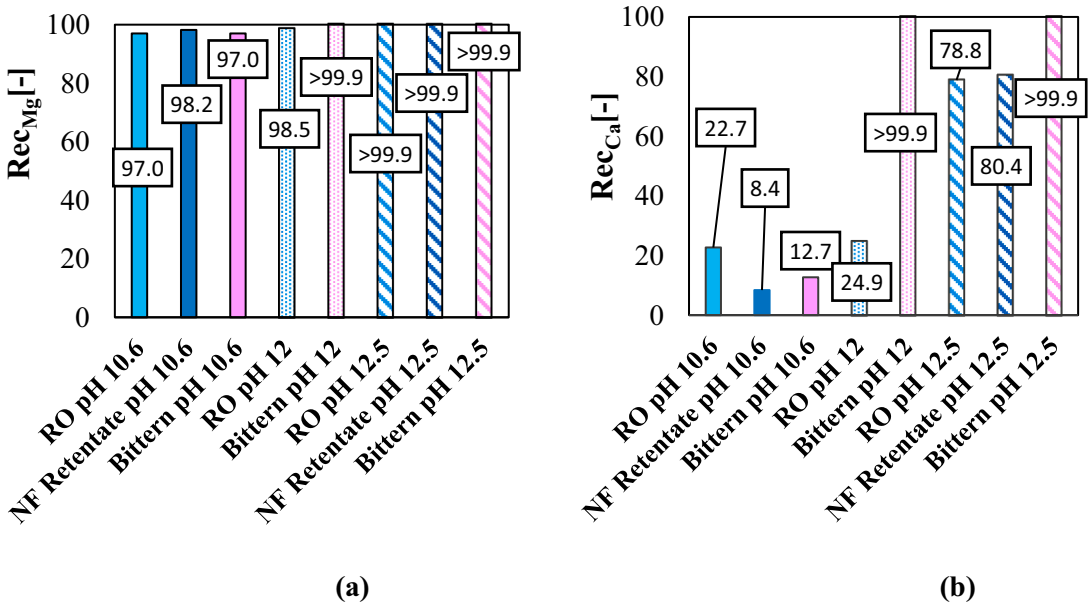

Fig. A7. Mg^{2+} (a) and Ca^{2+} (b) recoveries, Eq. (A.3) from RO brine, NF retentate and saltworks solutions at final pH values of 10.6, 12 and 12.5.

Magnesium ions recovery was above 97.0 % in all cases, reaching a value >99.9 % at pH values higher than 12.0 thanks to the large availability of OH^- ions in the reaction environment. At pH 10.6, calcium recoveries were 22.7 %, 8.4 % and 12.7 % for RO brine, NF retentate and bittern solutions, respectively. At pH of 12 Ca^{2+} recovery was 24.9 for RO brine, while a value >99.9 % was found for the bittern. Finally, at pH of 12.5, recovery values were ~ 80 % in RO brine and NF retentate cases, while again >99.9 % for the bittern. Results are in line with literature data [80]. Fig. A8 shows the cation purity of produced $Mg(OH)_2$ powders, Eq. (A.4).

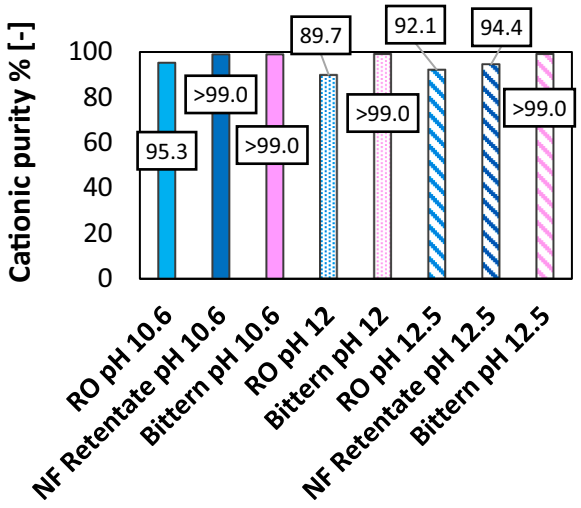

Fig. A8. Cationic purity of $Mg(OH)_2$ powders synthesized from RO brine, NF retentate and bittern solutions at pH values of 10.6, 12 and 12.5.

$Mg(OH)_2$ powders produced from bitterns had always a cationic purity >99 %. Note that, in the calculation the Limit of Quantification for Na^+ and Ca^{2+} were considered (3 mg/g and 1.3 mg/g, respectively). The high purity of the solids can be related to the low calcium content in the bittern, which precipitates in the saltworks through several evaporation ponds. The purity of the powders produced from the RO brine decreased from 95.3 to ~90.0 as the final pH of the suspension increased from 10.6 to 12.5, mainly due to the co-precipitation of $CaCO_3$. $Mg(OH)_2$ powders obtained from NF retentate solution exhibited a purity of 99 % at pH 10.6, while it decreased down to 94.4 % at the pH value of 12.5. Solids from NF retentate showed higher purity than those from RO brine due to the acidification of the NF treatment solution at the end of the NF step that can reduce the concentration of equivalent carbonates, see Section A.3.1. To further investigate the nature of the precipitated species, XRD spectra of solids are shown in Fig. A9.

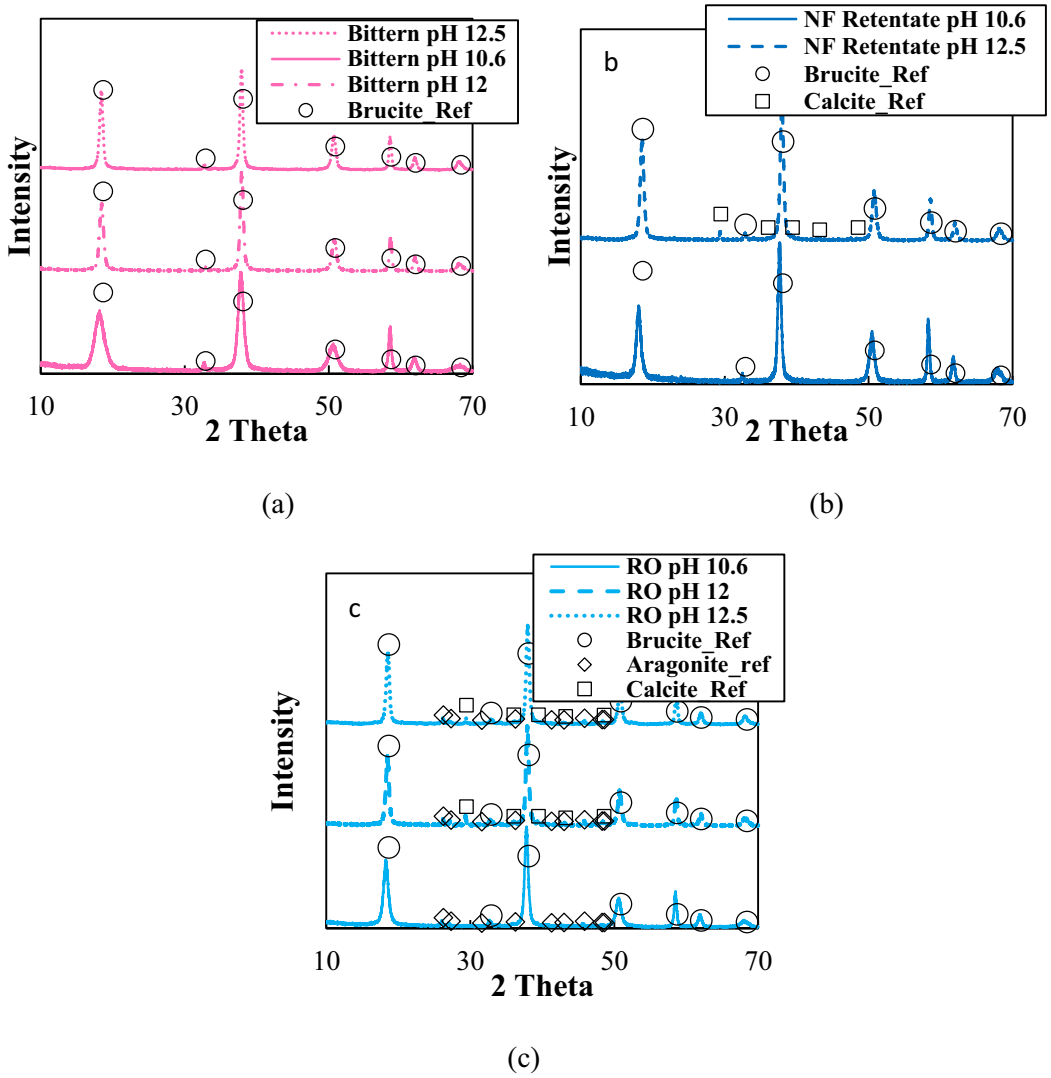

Fig. A9. XRD spectra of solids collected in $Mg(OH)_2$ tests from bittern (a), NF retentate (b), RO brine (c) at pH values of 10.6, 12 and 12.5. Reference spectra of brucite, aragonite and calcite species were taken from RRUFF™ database [81].

$Mg(OH)_2$, i.e., brucite, was the dominant phase in all solids. Samples from bittern solutions exhibited only peaks attributed to $Mg(OH)_2$ solids, thus indicating a high purity of the powders. Peaks of $CaCO_3$ species, in the form of aragonite and calcite, were detected in powders produced from RO brine and NF retentate, as reported by Battaglia et al. [82]. Specifically, $CaCO_3$ as calcite was identified in samples produced from the NF retentate solution at pH values of 12.5, while samples from RO brine exhibited the presence of aragonite at a pH value of 10.6 and the co-presence of aragonite and calcite at pH higher than 12. This is in accordance with the stability of polymorphisms of $CaCO_3$ at different pH values [83]. The presence of calcite was identified at peak at ~29.48, while peaks at ~26.24 and ~27.31 indicated the aragonite.

A.3.3. EDBM

Fig. A10 shows the time evolution of the OH^- concentration for the three clarified solutions collected at pH values of 10.6, 12 and 12.5, respectively.

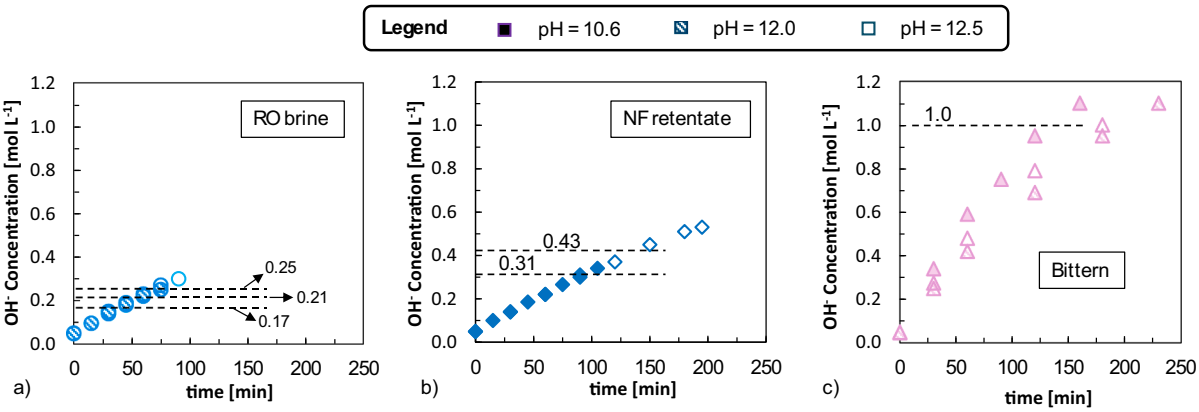

Fig. A10. OH^- concentration profiles along time for tests with clarified solutions after $Mg(OH)_2$ precipitation from a) RO brine, b) NF retentate and c) bittern solutions.

Different target concentrations, i.e. the OH^- concentrations adopted in $Mg(OH)_2$ precipitation testes, see Table A3, ranging between 0.17 mol/L and 1.0 mol/L were successfully achieved between 60 min and 180 min, proving the use of EDBM units in circular treatment chains for the efficient in-situ production of acidic and alkaline solutions. The required volume of the alkaline solutions was also produced. Overall, performances were in line with literature studies [38].

Fig. A11 reports Specific Energetic Consumption (*SEC*), Eq. (A.5), and Current Efficiency (*CE*), Eq. (A.6), for the different treated brines calculated at the desired target OH^- concentration.

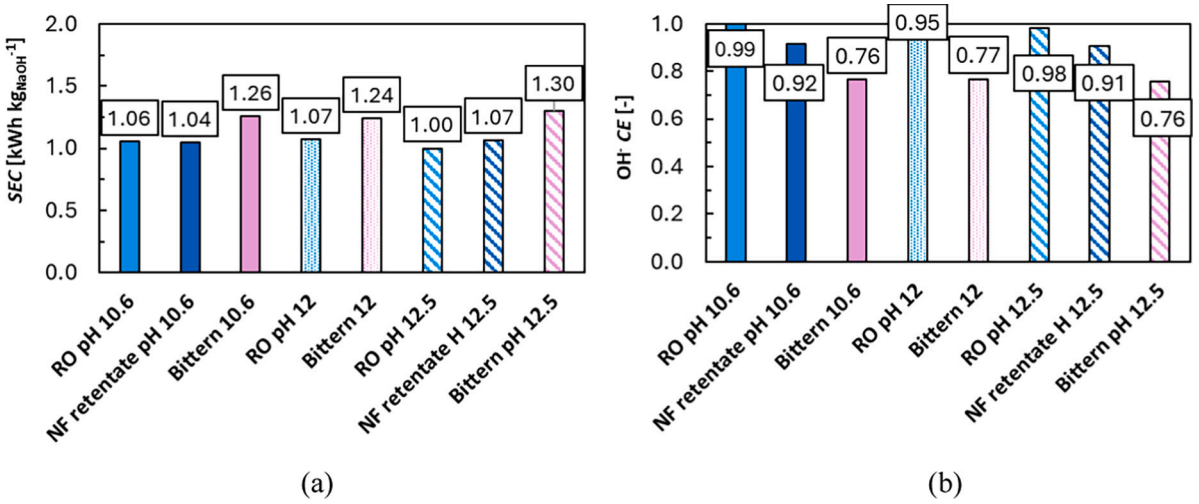

Fig. A11. a) Specific Energetic Consumption (*SEC*), Eq. (A.5), (b) Current Efficiency (*CE*), Eq. (A.6), for the different brines calculated at the desired OH^- concentration target.

The lowest *SEC* (~1.01–1.11 kWh/kg[1]) and the highest *CE* (~88–99 %) values were achieved in the tests with RO brine and NF retentate solutions, as the targeted alkaline concentrations were the lowest among the desired ones, i.e., in the range of 0.17–0.43 mol/L. In tests with bitterns, the need of more concentrated NaOH solutions resulted in higher energy consumption (up to 1.30 kWh/kg) and lower *CE* (up to 76 %). This can be related to a larger influence of undesired phenomena such as back diffusion and neutralization of H^+ and OH^-. Overall, *SEC* and *CE* values agreed well with literature findings [84,85].

A.3.4. Membrane distillation

Table A8 reports the electric conductivity measured at 25 °C of saline solutions before (outcoming the EDMB unit) and after the MD treatment.

Table A8
Electric conductivity (Cond.) at 25 °C of saline solutions before (outcoming the EDMB unit) and after the MD treatment.

	Initial *Cond.* (after EDBM unit) [mS/cm]	Final *Cond.* (after MD unit) [mS/cm]
Bittern	38.9	155.5
RO brine	20.5	129.3
NF retentate	39.6	155.7

Highly concentrated solutions were successfully produced even working at a relatively low temperature gradients (brines streams at 45 °C and distillate at 20 °C).

Fig. A12 shows the evolution of the distillate flux across the membrane during the tests as a function of the recovery rate, Eq. (A.8).

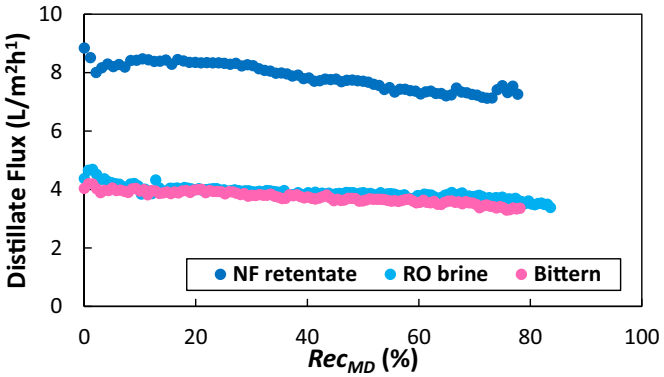

Fig. A12. Water vapor flux as a function of recovery factor for MD tests.

The distillate flux slightly decreased with increasing recovery factor. This behavior was expected due to fouling, scaling and polarizations phenomena, among the others [86,87]. Tests conducted with the smaller unit (140 cm^2, NF retentate case) exhibited higher fluxes than the RO brine and bittern ones. This was mainly due to the use of the smaller module, since MD scale-up applications typically result in a reduction of the distillate flux, mainly because greater membrane areas lead to higher conductive heat loss [89,90]. Overall, results are in accordance with literature data [91–93] highlighting the possibility of treating concentrated saline solutions with MD units. A recovery factor of approximately 80 % was achieved in all tests. However, higher recovery rates could be attained since no sign of membrane wetting (water passage through the membrane pores) was detected. Table A9 presents the average electric conductivity of the distillate, Eq. (A.7), and the corresponding rejection, calculated as shown in Eq. (A.9).

Table A9
Average electric conductivity values of collected distillates, c_d, and values of the average rejection calculated during the test.

	c_d, Eq. (A.7) [μS/cm]	Average rejection, Eq. (A.8) [%]
Bittern	6.25	99.98
RO brine	25.31	99.87
NF retentate	13.32	99.97

Once again, results confirmed the possibility to produce high quality fresh water by adopting the MD units to treat concentrated real solutions.

A.3.5. RED unit

Fig. A13 reports gross and net power density obtained in RED tests.

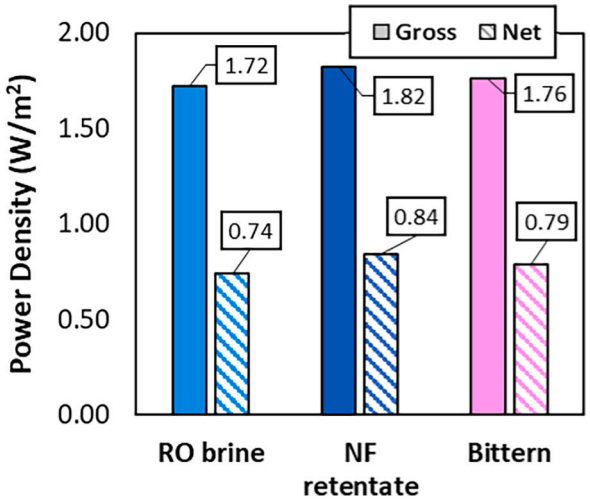

Fig. A13. $P_{d,gross}$ (solid bars) and $P_{d,net}$ (dashed bars), Eqs. (A.10) and (A.11), measured in RED tests. A reclaimed water was adopted as low saline solution for all tests. Flow velocities were 0.5 cm/s and 1.0 cm/s for high and low salinity solutions, respectively.

Similar $P_{d,gross}$ and $P_{d,net}$ values in the range of 1.72–1.82 W/m^2 and 0.74–0.84 W/m^2 were observed in all tests, being the net power density always positive. The highest values were attained with NF retentate and bittern solutions due to their initial higher conductivity, see Table *A8*. It must be highlighted that, due to the small number of cell pairs, the performances here obtained are expected to be largely affected by the resistance of electrode compartments. Referring to the concept of "corrected" net power density see [94], values would be ~4–5 W/m^2, in line with those reported in literature [95]. Overall, results demonstrate the potential of using RED units to harness high-salinity solutions for electrical energy generation and the use of reclaimed water to valorize waste product in circular approaches. Worth noting that, the use of different solution flow rates also allowed the concentration of the average saline solution to be close to that of seawater, thus effectively closing the chain.

Table A10 reports the values of stack resistance, R_{stack}, and cell pair resistance $R_{cell\ pair}$ in the performed tests.

Table A10
R_{stack} and $R_{cell\ pair}$ measured in performed tests.

	R_{stack} (Ω)	$R_{cell\ pair}$ (Ω)
Bittern	1.59	0.46
RO brine	1.59	0.46
NF retentate	1.61	0.47

Appendix B

B.1. Numerical model

To model real phenomena, such as magnesium conversion, ionic fluxes across the membranes or power generation in the RED unit, a statistical based-model analysis of the experimental data was conducted. For this purpose, the Pearson correlation coefficient, namely r_p, was employed. This coefficient is a widely used statistical tool for identifying relationships and dependencies between variables, particularly in experimental and observational contexts. The r_p coefficient, see Eq. (B1), quantifies the strength and direction of a linear relationship between two continuous variables.

$$r_p = \frac{\sum_{i=1}^{n}(X_i - \overline{X})(Y_i - \overline{Y})}{\sqrt{\sum_{i=1}^{n}(X_i - \overline{X})^2}\sqrt{\sum_{i=1}^{n}(Y_i - \overline{Y})^2}} \tag{B1}$$

where X_i and Y_i are individual sample point and $\overline{X}$, $\overline{Y}$ are the sample average of X and Y, and n is the number of samples.

The Pearson index ranges from −1 to +1, where a value close to +1 indicates a strong positive linear correlation (i.e., both variables increase together), while a value close to −1 indicates a strong negative linear correlation (i.e., one variable increases as the other decreases). A value near 0 suggests the absence of a linear correlation. It is important to note that Pearson's r is limited to linear relationships and does not capture nonlinear or more complex interactions between variables [96].

For each correlation, a p-value was determined to evaluate the probability of observing such a result if the null hypothesis was true [97]. The null hypothesis (H_o) is the default assumption of no correlation between variables or, in other words, that the true correlation is zero. A low p-value (typically <0.05) suggests that the result is unlikely under H_o, providing evidence against it and then confirming the real correlation between the two variables. In this study, only variables with p-values less than 0.05 were considered statistically significant.

B.2. Model calibration

Once the datasets were compiled with all the data collected by experimental tests and literature evidence, the Pearson coefficients and p-value indexes were evaluated. Statistical analysis was performed in Python 3.11 using Pandas and NumPy as library.

B.2.1. Magnesium hydroxide crystallizer

Data collected from the experimental trials and from other data present in the group database have been compiled into a single dataset, with entries categorized according to the type of input solution. The dataset consists of 63 rows and 7 columns [36,42]. The columns include the flowrates of brine/bittern and soda solution and their concentration, the soda over-stoichiometric flowrate, pH and magnesium conversion. Table B1 shows the statistical analysis conducted with this unit.

Table B1
Pearson coefficients and p values of the statistical analysis conducted for the reactive precipitation reactor.

Feed	Features	*Correlation*	r_p	*p value*
Bittern	pH	pH - %Exc soda	0.86	2.8 E−17
	Conversion	Conversion - pH	0.58	2.8 E−06
Brines	pH	pH - %Exc soda	0.98	3.0 E−03
	Conversion	Conversion - pH	0.90	3.7 E−02

The correlation values obtained indicate a clear relationship, for both solutions analyzed, i.e., bittern and brine, between the increase in soda flow rate (both sub-stoichiometric and over-stoichiometric conditions) and the corresponding increase in pH. Similar correlation indices were also found for the pH – conversion relationship. However, in this case, the indices are influenced by the natural distribution of the data points, which does not follow a monotonic trend but rather a typical saturation curve [36]. This behavior affects the analysis, especially when the pH reaches levels that lead to complete (unitary) conversion. Given the high correlation coefficient observed between pH and the percentage of excess soda (%Exc soda), a linear model was selected to fit this relationship. In contrast, the conversion data, due to its inherent behavior, was fitted using a saturation-type curve, which better captures the non-linear trend typically associated with such systems. Relationships are shown in Table B2.

Table B2
pH and magnesium conversion correlation low in the case of bittern and RO/NF brines.

Feed	Features	*Correlation Law*	R^2
Bittern	pH	$pH = 10.55 + 7.38\%Exc\ soda$	0.83

(*continued on next page*)

Table B2 (*continued*)

Feed	Features	*Correlation Law*	R^2
Brines	Mg conversion	$Conversion = \frac{1}{1+e^{-2.54(pH-9.64)}}$	0.84
	pH	$pH = 10.55 + 4.014\%Exc\ soda$	0.95
	Mg conversion	$Conversion = \frac{1}{1+e^{-3.17(pH-9.55)}}$	0.99

The correlations obtained for brine and bittern solutions clearly show that the regressed features exhibit similar trends in both cases. Notably, the regression coefficients are comparable, though slight differences can be observed, reflecting the distinct chemical nature of the two solutions. In the case of bittern, the complexity of the system, characterized by extremely high ionic concentrations, may give rise to specific effects that are not detectable in more diluted solutions, thereby leading to minor deviations in the regression models.

B.2.2. Electrodialysis with bipolar membranes (EDBM)

All EDBM data collected from the experimental trials have been compiled into a single dataset, with entries categorized according to the type of input solution. The dataset consists of 56 rows and 21 columns from the laboratory experimental data collection. Columns include the concentrations of key ions (Na^+, K^+, Cl^-, SO_4^{2-}, H^+, and OH^-) in the salt, acid, and base streams. Additionally, another column is dedicated to stack electrical resistance. Table B3 presents the Pearson correlation coefficients calculated for both the basic and acidic solutions by varying the inlet composition while Table B4 shows the corresponding *p*-value.

Table B3
Pearson's coefficient of EDBM features. Acid solution features are correlated to H^+ concentration in acid solution while base solution Features and stack resistances are correlated to OH- concentration in base solution.

	Acid solution [H^+]				Base solution [OH^-]			
	Na^+	K^+	Cl^-	SO_4^{2-}	Na^+	K^+	Cl^-	SO_4^{2-}
Brine	0.45	0.045	1	0.91	1	0.98	0.84	0.49
Bittern	0.89	0.67	0.99	0.87	0.99	0.98	0.66	0.67

Table B4
p-Value EDBM feature. Acid solution features are correlated to H+ concentration in acid solution while base solution features and stack resistances are correlated to OH- concentration in base solution.

	Acid solution [H^+]				Base solution [OH^-]			
	Na^+	K^+	Cl^-	SO_4^{2-}	Na^+	K^+	Cl^-	SO_4^{2-}
Brine	6E−3	8E−1	1E−37	8E−14	4E−36	4E−24	4E−10	3E−3
Bittern	1E−8	5E−4	3E−19	5E−8	7E−18	1E−15	6E−4	4E−4

The analysis confirms the existence of correlations that can be used to estimate the composition of the basic or acidic solution for a given target concentration of OH^- or H^+, respectively. It is evident that these correlations vary depending on the type of saline solution used (brine or bittern). A notable example concerns the presence of potassium in the acidic solution: it appears to be impossible to estimate in the case of brine (as indicated by a p-value of 0.8, suggesting randomness in the results), whereas in the case of bittern, where potassium is present at higher concentrations, a significant correlation emerges.

The correlation analysis shows Pearson coefficients with absolute values greater than or equal to 0.45 suggesting linear or monotonic relationship between variables. In the following table, Table B5, the adopted correlations were reported:

Table B5
EDBM correlation law and R^2 scores.

Feature	Correlation low	R^2
Na^+_{acid}[M]	$Na^+_{acid} = 0.0043 - 0.0045\cdot[H^+_{acid}] + 0.0492\cdot[H^+_{acid}]^2$	0.714
Cl^-_{acid}[M]	$Cl^-_{acid} = 0.0071 + 0.998\,[H^+_{acid}]$	0.986
SO_4^{2-} *acid*[M]	$SO_4^{2-}\ acid = 0.0531\,([H^+_{acid}])^{1.663}$	0.941
Na^+_{base}[M]	$Na^+_{base} = 0.0104 + 0.943\,[OH^-_{base}]$	0.983
K^+_{base}[M]	$K^+_{base} = 0.0001 + 0.0195\,[OH^-_{base}]$ (*for brine*)	0.956
	$K^+_{base} = 0.0004 + 0.066\,[OH^-_{base}]$ (*for bittern*)	0.954
Cl^-_{base}[M]	$Cl^-_{base} = 0.0011 + 0.0309\,[OH^-_{base}]$(*for brine*)	0.721
	$Cl^-_{base} = 0.0049 + 0.0286\,[OH^-_{base}] + 0.0213\,([OH^-_{base}])^2$ (*for bittern*)	0.903

Regressions exhibited satisfactory R^2 values, indicating a decent level of the fit of the model. For most of the variables related to brine and bittern, the observed trends are highly similar, justifying the use of a common regression law. Conversely, when the behavior of the variables diverges significantly, distinct regression models are employed to better capture their individual characteristics.

In general, an almost perfect linear correlation is observed between the respective counterions of OH^- and H^+, respectably Na^+ and Cl^-. However,

the correlations become less linear when considering the co-ions (such as K^+ or SO_4^{2-}), and even more in the presence of ions that migrate due to diffusion or non-ideal phenomena, such as Na^+ in the acid or Cl^- in the base. Another key parameter in the operation of the EDBM unit is the stack resistance, which is defined as the total electrical resistance of the system. The stack resistance is not a fixed value; it varies significantly with the ionic composition of the solutions circulating within the unit and strongly depends on the concentration of ions in each compartment. Due to the limited amount of experimental data collected during the experimental campaign, the initial resistance values of the EDBM unit, which are the highest values over the EDBM functioning, provided by the experimental data, were adopted, thus numerical results provide over-estimated EnEx values for the EDBM unit. The referenced stack resistance value R_{stack} is presented in Table B6.

Table B6
Stack resistance values of the EDBM unit adopted in the model.

	RO brine	NF ret	Bittern
$R_{stack}\left[\Omega cm^2\right]$	64.12	62.61	60.97

Data availability

Data will be made available on request.

References

[1] H. Ritchie, L. Rodés-Guirao, Peak global population and other key findings from the 2024 UN World Population Prospects, Our World in Data, 2024. https://ourworldindata.org/un-population-2024-revision. (Accessed 8 May 2025).

[2] J. Kim, S. Hong, A novel single-pass reverse osmosis configuration for high-purity water production and low energy consumption in seawater desalination, Desalination 429 (2018) 142–154, https://doi.org/10.1016/J.DESAL.2017.12.026.

[3] L.F. Greenlee, D.F. Lawler, B.D. Freeman, B. Marrot, P. Moulin, Reverse osmosis desalination: water sources, technology, and today's challenges, Water Res. 43 (2009) 2317–2348, https://doi.org/10.1016/J.WATRES.2009.03.010.

[4] M. Clever, F. Jordt, R. Knauf, N. Räbiger, M. Ruedebusch, R. Hilker-Scheibel, Process water production from river water by ultrafiltration and reverse osmosis, Desalination 131 (2000) 325–336, https://doi.org/10.1016/S0011-9164(00)90031-6.

[5] M. Turek, Dual-purpose desalination-salt production electrodialysis, Desalination 153 (2003) 377–381, https://doi.org/10.1016/S0011-9164(02)01131-1.

[6] T. Sirivedhin, J. McCue, L. Dallbauman, Reclaiming produced water for beneficial use: salt removal by electrodialysis, J. Membr. Sci. 243 (2004) 335–343, https://doi.org/10.1016/J.MEMSCI.2004.06.038.

[7] A. Khouya, Performance evaluation of a MED-MVC desalination plant driven by a concentrated photovoltaic thermal system and an organic Rankine cycle, Energ. Conver. Manage. 274 (2022) 116428, https://doi.org/10.1016/J.ENCONMAN.2022.116428.

[8] J.J. Feria-Díaz, M.C. López-Méndez, J.P. Rodríguez-Miranda, L.C. Sandoval-Herazo, F. Correa-Mahecha, Commercial thermal technologies for desalination of water from renewable energies: a state of the art review, Processes 9 (2021) 262, https://doi.org/10.3390/PR9020262.

[9] L.M. Camacho, L. Dumée, J. Zhang, J. de Li, M. Duke, J. Gomez, S. Gray, Advances in membrane distillation for water desalination and purification applications, Water (Switzerland) 5 (2013) 94–196. doi:https://doi.org/10.3390/W5010094.

[10] M.P. Godino, L. Peña, C. Rincón, J.I. Mengual, Water production from brines by membrane distillation, Desalination 108 (1997) 91–97, https://doi.org/10.1016/S0011-9164(97)00013-1.

[11] D. Curto, V. Franzitta, A. Guercio, A review of the water desalination technologies, Appl. Sci. 2021, Vol. 11, Page 670 11 (2021) 670. doi:https://doi.org/10.3390/APP11020670.

[12] S.S. Mousavi, A. Kargari, Water recovery from reverse osmosis concentrate by commercial nanofiltration membranes: a comparative study, Desalination 528 (2022) 115619, https://doi.org/10.1016/J.DESAL.2022.115619.

[13] D. Xevgenos, M. Marcou, V. Louca, E. Avramidi, G. Ioannou, M. Argyrou, P. Stavrou, M. Mortou, F.C. Küpper, Aspects of environmental impacts of seawater desalination: Cyprus as a case study, Desalin. Water Treat. 211 (2021) 15–30, https://doi.org/10.5004/dwt.2021.26916.

[14] S. Uddin, Environmental impacts of desalination activities in the Arabian Gulf, Int. J. Environ. Sci. Dev. (2014) 114–117, https://doi.org/10.7763/ijesd.2014.v5.461.

[15] S. Randazzo, F. Vicari, J. López, M. Salem, R. Lo Brutto, S. Azzouz, S. Chamam, S. Cataldo, N. Muratore, M. Fernández de Labastida, V. Vallès, A. Pettignano, G. D'Alì Staiti, S. Pawlowski, A. Hannachi, J.L. Cortina, A. Cipollina, Unlocking hidden mineral resources: characterization and potential of bitterns as alternative sources of critical raw materials, J. Clean. Prod. 436 (2024) 140412, https://doi.org/10.1016/j.jclepro.2023.140412.

[16] F. Vicari, S. Randazzo, J. López, M. Fernández de Labastida, V. Vallès, G. Micale, A. Tamburini, G. D'Alì Staiti, J.L. Cortina, A. Cipollina, Mining minerals and critical raw materials from bittern: understanding metal ions fate in saltwork ponds, Sci. Total Environ. 847 (2022) 157544, https://doi.org/10.1016/J.SCITOTENV.2022.157544.

[17] H. Abdel-Aal, K. Zohdy, M.A. Kareem, Separation of Magnesium Chloride from Sea Water by Preferential Salt Separation (PSS), Tenth of ramadan, Egypt, 2013. https://www.researchgate.net/publication/281508759.

[18] S.A. Neves, A.C. Marques, Drivers and barriers in the transition from a linear economy to a circular economy, J. Clean. Prod. 341 (2022) 130865, https://doi.org/10.1016/J.JCLEPRO.2022.130865.

[19] A.P.M. Velenturf, P. Purnell, Principles for a sustainable circular economy, Sustain. Prod. Consum. 27 (2021) 1437–1457, https://doi.org/10.1016/J.SPC.2021.02.018.

[20] Circular Processing of Seawater Brines from Saltworks for Recovery of Valuable Raw Materials - SEArcular Mine, (n.d.). https://searcularmine.eu/ (accessed August 27, 2024).

[21] V. Vallès, M.F. de Labastida, J. López, J.L. Cortina, Selective recovery of boron, cobalt, gallium and germanium from seawater solar saltworks brines using N-methylglucamine sorbents: column operation performance, Sci. Total Environ. 923 (2024) 171438, https://doi.org/10.1016/j.scitotenv.2024.171438.

[22] A. Yoshida, R. Komatsu, A mechanism for reducing the specific surface area of polycrystalline magnesium hydroxide, J. Ceram. Soc. Japan 117 (2009) 1166–1171.

[23] J. Nie, S.Z. Yi, Neutralization of acid wastewater and magnesium hydroxide slurry from seawater electrolytic pretreatment, Adv. Mat. Res. 1073–1076 (2014) 949–954, https://doi.org/10.4028/WWW.SCIENTIFIC.NET/AMR.1073-1076.949.

[24] R. Giorgi, C. Bozzi, L. Dei, C. Gabbiani, B.W. Ninham, P. Baglioni, Nanoparticles of Mg(OH)2: synthesis and application to paper conservation, Langmuir 21 (2023) 8495–8501, https://doi.org/10.1021/LA050564M.

[25] T. Li, T.C. Keener, L. Cheng, Carbon dioxide removal by using Mg(OH)2 in a bubble column: effects of various operating parameters, Int. J. Greenhouse Gas Control 31 (2014) 67–76, https://doi.org/10.1016/J.IJGGC.2014.09.027.

[26] B.A. Abdelkader, M.A. Antar, Z. Khan, Nanofiltration as a pretreatment step in seawater desalination: a review, Arab. J. Sci. Eng. 43 (2018) 4413–4432, https://doi.org/10.1007/S13369-018-3096-3.

[27] C. Morgante, F. Vassallo, C. Cassaro, G. Virruso, D. Diamantidou, N. Van Linden, A. Trezzi, C. Xenogianni, R. Ktori, M. Rodriguez, G. Scelfo, S. Randazzo, A. Tamburini, A. Cipollina, G. Micale, D. Xevgenos, Pioneering minimum liquid discharge desalination: a pilot study in Lampedusa Island, Desalination 581 (2024) 117562, https://doi.org/10.1016/J.DESAL.2024.117562.

[28] F. Vassallo, D. La Corte, N. Cancilla, A. Tamburini, M. Bevacqua, A. Cipollina, G. Micale, A pilot-plant for the selective recovery of magnesium and calcium from waste brines, Desalination 517 (2021) 115231, https://doi.org/10.1016/J.DESAL.2021.115231.

[29] G. Virruso, C. Cassaro, F. Vassallo, A. Filingeri, A. Pellegrino, A. Tamburini, A. Cipollina, G.D.M. Micale, A pilot plant investigation on a real seawater brine valorisation via electrodialysis with bipolar membranes, J Water Process Eng 69 (2025) 106741, https://doi.org/10.1016/j.jwpe.2024.106741.

[30] Y.C. Woo, S.H. Kim, H.K. Shon, L.D. Tijing, Introduction: Membrane desalination today, past, and future, in: Current Trends and Future Developments on (Bio-) Membranes: Membrane Desalination Systems: The Next Generation, 2018, pp. xxv–xlvi, https://doi.org/10.1016/B978-0-12-813551-8.00028-0.

[31] M.G. Buonomenna, Membranes for blue energy conversion by reverse electrodialysis (RED), in: Nano-enhanced and Nanostructured Polymer-based Membranes for Energy Applications, 2022, pp. 91–137, https://doi.org/10.1016/B978-0-08-101985-6.00001-X.

[32] V.T. Luong, R. Amal, J.A. Scott, S. Ehrenberger, T. Tran, A comparison of carbon footprints of magnesium oxide and magnesium hydroxide produced from conventional processes, J. Clean. Prod. 202 (2018) 1035–1044, https://doi.org/10.1016/J.JCLEPRO.2018.08.225.

[33] M.A. Tribe, R.L.W. Alpine, Scale economies and the "0.6 rule,", Eng. Costs Prod. Econ. 10 (1986) 271–278, https://doi.org/10.1016/S0167-188X(86)80025-8.

[34] C. Kaya, Y.A. Jarma, A.M. Muhidin, E. Güler, N. Kabay, M. Arda, M. Yüksel, Seawater desalination by using nanofiltration (NF) and brackish water reverse osmosis (BWRO) membranes in sequential mode of operation, J. Membr. Sci. Res. 6 (2020) 40–46, https://doi.org/10.22079/JMSR.2019.107844.1264.

[35] Ksp Table, (n.d.). https://owl.oit.umass.edu/departments/Chemistry/appendix/ksp.html (accessed July 24, 2025).

[36] L. Ventimiglia, F. Vassallo, G. Lo Burgio, A. Campione, L. Cammilli, P. Vicario, G. Battaglia, F. Vicari, A. Cipollina, A. Tamburini, G. Micale, Pilot scale production of Mg(OH)2 compounds from a real industrial reverse osmosis desalination brine, Desalination 613 (2025), https://doi.org/10.1016/J.DESAL.2025.119052.
[37] Purolite™ Shallow Shell™ SSTC104, (n.d.). https://www.purolite.com/product?normalizedName=sstc104 (accessed May 29, 2025).
[38] A. Filingeri, A. Culcasi, M. Nanfara, C. Cassaro, A. Tamburini, G. Micale, A. Cipollina, Exploring differential pressure-induced hydraulic flows in pilot-scale Electrodialysis with bipolar membranes, J. Environ. Manage. 373 (2025) 123538, https://doi.org/10.1016/J.JENVMAN.2024.123538.
[39] L. Eykens, I. Hitsov, K. De Sitter, C. Dotremont, L. Pinoy, B. Van der Bruggen, Direct contact and air gap membrane distillation: differences and similarities between lab and pilot scale, Desalination 422 (2017) 91–100, https://doi.org/10.1016/J.DESAL.2017.08.018.
[40] D. Rowland, E. Königsberger, G. Hefter, P.M. May, Aqueous electrolyte solution modelling: some limitations of the Pitzer equations, Appl. Geochem. 55 (2015) 170–183, https://doi.org/10.1016/J.APGEOCHEM.2014.09.021.
[41] M. Amouamouha, G.B. Gholikandi, M. Amouamouha, G. Badalians Gholikandi, Performance investigation and cost evaluation of nanofiltration membranes in groundwater remediation, in: International Conference on Small and Decentralized Water and Wastewater Treatment Plants, 5th ed., 2018 (Thessaloniki; https://www.researchgate.net/publication/341984702).
[42] G. Scelfo, V.M. Charitopoulos, F. Vicari, A. Tamburini, D.I. Bogle, G. Micale, A. Cipollina, Surrogate-based optimization analysis and scale-up of an ultra-concentrated brine pilot treatment chain for sustainable mineral recovery, Desalination 621 (1 March 2026) 119682, https://doi.org/10.1016/j.desal.2025.119682.
[43] S. He, X. Zhang, X. Xia, C. Wang, S. Xiang, Low energy consumption electrically regenerated ion-exchange for water desalination, Water Sci. Technol. 82 (2020) 1710–1719, https://doi.org/10.2166/WST.2020.442.
[44] Y.J. Choi, S. Lee, J. Koo, S.H. Kim, Evaluation of economic feasibility of reverse osmosis and membrane distillation hybrid system for desalination, desalination water treat 57 (2016) 24662–24673, https://doi.org/10.1080/19443994.2016.1152648.
[45] D. Winter, J. Koschikowski, F. Gross, D. Maucher, D. Düver, M. Jositz, T. Mann, A. Hagedorn, Comparative analysis of full-scale membrane distillation contactors - methods and modules, J. Membr. Sci. 524 (2017) 758–771, https://doi.org/10.1016/J.MEMSCI.2016.11.080.
[46] M. Tedesco, A. Cipollina, A. Tamburini, G. Micale, Towards 1 kW power production in a reverse electrodialysis pilot plant with saline waters and concentrated brines, J. Membr. Sci. 522 (2017) 226–236, https://doi.org/10.1016/J.MEMSCI.2016.09.015.
[47] J.Y. Nam, K.S. Hwang, H.C. Kim, H. Jeong, H. Kim, E. Jwa, S.C. Yang, J. Choi, C. S. Kim, J.H. Han, N. Jeong, Assessing the behavior of the feed-water constituents of a pilot-scale 1000-cell-pair reverse electrodialysis with seawater and municipal wastewater effluent, Water Res. 148 (2019) 261–271, https://doi.org/10.1016/J.WATRES.2018.10.054.
[48] M. Hardikar, I. Marquez, T. Phakdon, A.E. Sáez, A. Achilli, Scale-up of membrane distillation systems using bench-scale data, Desalination 530 (2022) 115654, https://doi.org/10.1016/J.DESAL.2022.115654.
[49] V.R. Moreira, J.V. Raad, J.X. Lazarini, L.V.S. Santos, M.C.S. Amaral, Recent progress in membrane distillation configurations powered by renewable energy sources and waste heat, J Water Process Eng 53 (2023) 103816, https://doi.org/10.1016/J.JWPE.2023.103816.
[50] A. Cipollina, M.G. Di Sparti, A. Tamburini, G. Micale, Development of a membrane distillation module for solar energy seawater desalination, Chem. Eng. Res. Des. 90 (2012) 2101–2121, https://doi.org/10.1016/J.CHERD.2012.05.021.
[51] S.O. Olatunji, L.M. Camacho, Heat and mass transport in modeling membrane distillation configurations: a review, Front. Energy Res. 6 (2018) 421215, https://doi.org/10.3389/FENRG.2018.00130/FULL.
[52] A. Anvari, A. Azimi Yancheshme, K.M. Kekre, A. Ronen, State-of-the-art methods for overcoming temperature polarization in membrane distillation process: a review, J. Membr. Sci. 616 (2020) 118413, https://doi.org/10.1016/J.MEMSCI.2020.118413.
[53] T. Horseman, Y. Yin, K.S.S. Christie, Z. Wang, T. Tong, S. Lin, Wetting, scaling, and fouling in membrane distillation: state-of-the-art insights on fundamental mechanisms and mitigation strategies, ACS ES&T Engineering 1 (2020) 117–140, https://doi.org/10.1021/ACSESTENGG.0C00025.
[54] M. Gryta, Long-term performance of membrane distillation process, J. Membr. Sci. 265 (2005) 153–159, https://doi.org/10.1016/J.MEMSCI.2005.04.049.
[55] E. Guillén-Burrieza, G. Zaragoza, S. Miralles-Cuevas, J. Blanco, Experimental evaluation of two pilot-scale membrane distillation modules used for solar desalination, J. Membr. Sci. 409–410 (2012) 264–275, https://doi.org/10.1016/J.MEMSCI.2012.03.063.
[56] J. Choi, J. Cho, J. Shin, H. Cha, J. Jung, K.G. Song, Performance and economic analysis of a solar membrane distillation pilot plant under various operating conditions, Energ. Conver. Manage. 268 (2022) 115991, https://doi.org/10.1016/J.ENCONMAN.2022.115991.
[58] F. Volpe, E. Mangiaracina, G. Battaglia, A. Cipollina, G. Micale, A. Tamburini, Experimental analysis of an upscaled reverse electrodialysis unit featuring electrode segmentation, Sep. Purif. Technol. 382 (2026) 135857, https://doi.org/10.1016/J.SEPPUR.2025.135857.
[59] M. Tedesco, C. Scalici, D. Vaccari, A. Cipollina, A. Tamburini, G. Micale, Performance of the first reverse electrodialysis pilot plant for power production from saline waters and concentrated brines, J. Membr. Sci. 500 (2016) 33–45, https://doi.org/10.1016/J.MEMSCI.2015.10.057.
[60] Electricity price statistics - Statistics Explained - Eurostat, (n.d.). https://ec.europa.eu/eurostat/statistics-explained/index.php?title=Electricity_price_statistics (accessed May 15, 2025).
[62] J. Feo-García, A. Pulido-Alonso, A. Florido-Betancor, N.R. Florido-Suárez, Cost studies of reverse osmosis desalination plants in the range of 23,000–33,000 m3/day, Water 16 (6) (2024) 910, https://doi.org/10.3390/W16060910.
[63] Hydrochloric Acid Price - Historical & Current | Intratec.us, (n.d.). https://www.intratec.us/solutions/primary-commodity-prices/commodity/hydrochloric-acid-prices (accessed July 29, 2025).
[64] F. Beyer, J. Laurinonyte, A. Zwijnenburg, A.J.M. Stams, C.M. Plugge, Membrane fouling and chemical cleaning in three full-scale reverse osmosis plants producing demineralized water, J. Eng. 2017 (2017) 6356751, https://doi.org/10.1155/2017/6356751.
[65] M. Micari, M. Moser, A. Cipollina, A. Tamburini, G. Micale, V. Bertsch, Towards the implementation of circular economy in the water softening industry: a technical, economic and environmental analysis, J. Clean. Prod. 255 (2020) 120291, https://doi.org/10.1016/J.JCLEPRO.2020.120291.
[66] G. Scelfo, A. Trezzi, F. Vassallo, A. Cipollina, V. Landi, C. Xenogianni, A. Tamburini, D. Xevgenos, G. Micale, Demonstration of ultra-high-water recovery and brine concentration in a prototype evaporation unit: towards zero liquid discharge desalination, Sep. Purif. Technol. 354 (2025) 129427, https://doi.org/10.1016/j.seppur.2024.129427.
[67] M. Annamalai, T. Kannappan, Experimental studies on solar multi - effect sea water desalination system, Sol. Energy 259 (2023) 246–256, https://doi.org/10.1016/j.solener.2023.05.004.
[68] X. Zhang, Solar driven desalination system for power and desalination water production by concentrated PVT and MED system, Chem. Prod. Process. Model. (2023). doi:https://doi.org/10.1515/cppm-2023-0044, Chem. Prod. Process Model.
[69] G. Battaglia, L. Ventimiglia, F.P.M. Viggiano, F. Vassallo, A. Cipollina, A. Tamburini, G. Micale, Mg(OH)2 recovery from real bitterns: a proof of concept at pilot scale, Chem. Eng. Trans. 105 (2023) 1–6. doi:https://doi.org/10.3303/CET23105001.
[70] Veolia's Ion Exchange Membranes | Veolia WTS, (n.d.). https://www.watertechnologies.com/products/ion-exchange-membranes (accessed August 1, 2025).
[71] J. Moreno, S. Grasman, R. Van Engelen, K. Nijmeijer, Upscaling reverse electrodialysis, Environ. Sci. Technol. 52 (2018) 10856–10863, https://doi.org/10.1021/ACS.EST.8B01886/ASSET/IMAGES/LARGE/ES-2018-01886B_0005.JPEG.
[72] S.F. Corsino, D. Di Trapani, M. Torregrossa, G. Viviani, Aerobic granular sludge treating high strength citrus wastewater: analysis of pH and organic loading rate effect on kinetics, performance and stability, J. Environ. Manage. 214 (2018) 23–35, https://doi.org/10.1016/J.JENVMAN.2018.02.087.
[73] C. Lucia, V.A. Laudicina, L. Badalucco, A. Galati, E. Palazzolo, M. Torregrossa, G. Viviani, S.F. Corsino, Challenges and opportunities for citrus wastewater management and valorisation: a review, J. Environ. Manage. 321 (2022), https://doi.org/10.1016/j.jenvman.2022.115924.
[74] M. Tedesco, A. Cipollina, A. Tamburini, G. Micale, J. Helsen, M. Papapetrou, REAPower: use of desalination brine for power production through reverse electrodialysis, Desalin. Water Treat. 53 (2015) 3161–3169, https://doi.org/10.1080/19443994.2014.934102.
[75] L. Zheng, H. Zhong, Y. Wang, N. Duan, M. Ulbricht, Q. Wu, B. Van der Bruggen, Y. Wei, Mixed scaling patterns and mechanisms of high-pressure nanofiltration in hypersaline wastewater desalination, Water Res. 250 (2024) 121023, https://doi.org/10.1016/J.WATRES.2023.121023.
[76] A. Pérez-González, R. Ibáñez, P. Gómez, A.M. Urtiaga, I. Ortiz, J.A. Irabien, Nanofiltration separation of polyvalent and monovalent anions in desalination brines, J. Membr. Sci. 473 (2015) 16–27, https://doi.org/10.1016/J.MEMSCI.2014.08.045.
[77] J.A. Otero, G. Lena, J.M. Colina, P. Prádanos, F. Tejerina, A. Hernández, Characterisation of nanofiltration membranes: structural analysis by the DSP model and microscopical techiques, J Memb Sci 279 (2006) 410–417. doi:https://doi.org/10.1016/J.MEMSCI.2005.12.031, J. Membr. Sci.
[78] S. Bandini, J. Drei, D. Vezzani, The role of pH and concentration on the ion rejection in polyamide nanofiltration membranes, J. Membr. Sci. 264 (2005) 65–74, https://doi.org/10.1016/J.MEMSCI.2005.03.054.
[79] B. Van der Bruggen, Nanofiltration, in: encyclopedia of Membr. Sci. Technol., 2013, pp. 1–23, https://doi.org/10.1002/9781118522318.EMST077.
[80] G. Battaglia, M.A. Domina, R. Lo Brutto, J. Lopez Rodriguez, M. Fernandez de Labastida, J.L. Cortina, A. Pettignano, A. Cipollina, A. Tamburini, G. Micale, Evaluation of the purity of magnesium hydroxide recovered from saltwork bitterns, Water 15 (2023), https://doi.org/10.3390/W15010029.
[81] B. Lafuente, R.T. Downs, H. Yang, N. Stone, The power of databases: the RRUFF project, in: Highlights in Mineralogical Crystallography, 2016, pp. 1–29, https://doi.org/10.1515/9783110417104-003.
[82] G. Battaglia, M. Cardella, A. Tamburini, A. Cipollina, G. Micale, Exploitation of seawater brines for the production of Nesquehonite solids and CO2 utilization, J CO_2 Util 96 (2025) 103101, https://doi.org/10.1016/J.JCOU.2025.103101.
[83] F. Liendo, M. Arduino, F.A. Deorsola, S. Bensaid, Factors controlling and influencing polymorphism, morphology and size of calcium carbonate synthesized through the carbonation route: a review, Powder Technol. 398 (2022) 117050, https://doi.org/10.1016/J.POWTEC.2021.117050.
[84] A. Filingeri, J. Lopez, A. Culcasi, T. Leon, A. Tamburini, J. Luis Cortina, G. Micale, A. Cipollina, In-depth insights on multi-ionic transport in Electrodialysis with bipolar membrane systems, Chem. Eng. J. 468 (2023) 143673, https://doi.org/10.1016/j.cej.2023.143673.

[85] H. Tang, X. Wang, X. Zhao, Y. Dong, B. Xu, L. Wang, Ion migration characteristics during the bipolar membrane electrodialysis treatment of concentrated reverse osmosis brine, Desalination 561 (2023), https://doi.org/10.1016/j.desal.2023.116660.
[86] J. Qi, J. Lv, W. Bian, J. Li, S. Liu, Experimental study on the membrane distillation of highly mineralized mine water, Int. J. Coal Sci. Technol. 8 (2021) 1025–1033, https://doi.org/10.1007/S40789-021-00432-6/TABLES/4.
[87] D.M. Warsinger, J. Swaminathan, E. Guillen-Burrieza, H.A. Arafat, J.H. Lienhard V, Scaling and fouling in membrane distillation for desalination applications: a review, Desalination 356 (2015) 294–313, https://doi.org/10.1016/J.DESAL.2014.06.031.
[89] M. Khayet, Membranes and theoretical modeling of membrane distillation: a review, Adv. Colloid Interface Sci. 164 (2011) 56–88, https://doi.org/10.1016/J.CIS.2010.09.005.
[90] L.M. Camacho, L. Dumée, J. Zhang, J. de Li, M. Duke, J. Gomez, S. Gray, Advances in membrane distillation for water desalination and purification applications, Water 2013, Vol. 5, Pages 94–196 5 (2013) 94–196. doi:https://doi.org/10.3390/W5010094.
[91] M. Malaguti, L.K. Presson, A. Tiraferri, K.L. Hickenbottom, A. Achilli, Productivity, selectivity, and energy consumption of pilot-scale vacuum assisted air-gap membrane distillation for the desalination of high-salinity streams, Desalination 582 (2024), https://doi.org/10.1016/j.desal.2024.117511.
[92] M. Quilaqueo, G. Seriche, L. Barros, C. González, J. Romero, R. Ruby-Figueroa, S. Santoro, E. Curcio, H. Estay, Water recovery assessment from hypersaline lithium-rich brines using membrane distillation-crystallization, Desalination 537 (2022), https://doi.org/10.1016/j.desal.2022.115887.
[93] L. Wang, X. Sun, F. Gao, Y. Yang, R. Song, Solar membrane distillation: an emerging technology for reverse osmosis concentrated brine treatment, Desalination 592 (2024), https://doi.org/10.1016/j.desal.2024.118124.
[94] M. Tedesco, E. Brauns, A. Cipollina, G. Micale, P. Modica, G. Russo, J. Helsen, Reverse electrodialysis with saline waters and concentrated brines: a laboratory investigation towards technology scale-up, J. Memb. Sci. 492 (2015) 9–20, https://doi.org/10.1016/J.MEMSCI.2015.05.020.
[95] R.A. Tufa, S. Pawlowski, J. Veerman, K. Bouzek, E. Fontananova, G. di Profio, S. Velizarov, J. Goulão Crespo, K. Nijmeijer, E. Curcio, Progress and prospects in reverse electrodialysis for salinity gradient energy conversion and storage, Appl. Energy 225 (2018) 290–331, https://doi.org/10.1016/J.APENERGY.2018.04.111.
[96] A. Rebekić, Z. Lončarić, S. Petrović, S. Marić, Pearsonov ili spearmanov koeficijent korelacije - Koji koristiti? Poljoprivreda 21 (2015) 47–54, https://doi.org/10.18047/POLJO.21.2.8.
[97] C. Andrade, The p value and statistical significance: misunderstandings, explanations, challenges, and alternatives, Indian J. Psychol. Med. 41 (2019) 210, https://doi.org/10.4103/IJPSYM.IJPSYM_193_19.